FMU Rep. V 2
(DECEMBER 1973)

INDIA METEOROLOGICAL DEPARTMENT

FORECASTING MANUAL

PART V

TECHNIQUES OF HIGH LEVEL ANALYSIS AND PROGNOSIS

2 PROGNOSTIC TECHNIQUES AND ASSESSMENT OF ACCURACY OF FORECASTS

BY

P. K. DAS, N. C. RAI SIRCAR AND D. V. RAO.

ISSUED BY

DEPUTY DIRECTOR GENERAL OF OBSERVATORIES
(FORECASTING)
POONA-5

FORECASTING MANUAL REPORTS

No. I-1	Monthly Mean Sea Level Isobaric Charts – R.Ananthakrishnan, V. Srinivasan and A.R. Ramakrishnan.
No. I-2	Climate of India – Y.P. Rao and K.S. Ramamurti.
No. II-1	Methods of Analysis: 1. Map Projections for Weather Charts – K. Krishna.
No. II-4	Methods of Analysis: 4. Analysis of Wind Field – R.N.Keshavamurthy.
No. III-1.1	Discussion of Typical Synoptic Weather Situations: Winter – Western Disturbances and their Associated Features – Y.P. Rao and V. Srinivasan.
No. III-3.1	Discussion of Typical Synoptic Weather Situations: Southwest Monsoon: Active and Weak Monsoon conditions over Gujarat State – Y.P. Rao, V. Srinivasan, S.Raman and A.R.Ramakrishnan.
No. III-3.2	Discussion of Typical Synoptic Weather Situations: Southwest Monsoon: Active and Weak Monsoon conditions over Orissa – Y.P. Rao, V. Srinivasan, A.R.Ramakrishnan and S. Raman.
No. III-3.3	Discussion of Typical Synoptic Weather Situations: Southwest Monsoon: Typical Situations over Northwest India – M.S.V. Rao, V. Srinivasan and S. Raman.
No. III-3.4	Discussion of Typical Synoptic Weather Situations: Southwest Monsoon: Typical Situations over Madhya Pradesh and Vidarbha – V. Srinivasan, S. Raman and S. Mukherji.
No. III-3.5	Discussion of Typical Synoptic Weather Situations: Southwest Monsoon: Typical Situations over Uttar Pradesh and Bihar – V. Srinivasan, S. Raman and S. Mukherji.
No. III-3.6	Discussion of Typical Synoptic Weather Situations: Southwest Monsoon: Typical Situations over West Bengal and Assam and adjacent States – V. Srinivasan, S. Raman and S. Mukherji.
No. III-3.7	Discussion of Typical Synoptic Weather Situations: Southwest Monsoon: Typical Situations over Konkan and Coastal Mysore – V. Srinivasan, S. Raman, S. Mukherji and K. Ramamurthy.
No. III-3.8	Discussion of Typical Synoptic Weather Situations: Southwest Monsoon: Typical Situations over Kerala and Arabian Sea Islands – V. Srinivasan, S. Mukherji and K. Ramamurthy.
No. III-3.9	Discussion of Typical Synoptic Weather Situations: Southwest Monsoon: Typical Situations over Interior Peninsula and Coastal Andhra Pradesh – N.M. Philip, V. Srinivasan and K. Ramamurthy.

(Contd. on back cover page)

FMU Rep.No. V - 2
(December 1973)

FORECASTING MANUAL

Part V – Techniques of High Level Analysis and Prognosis

2. Prognostic Techniques and Assessment of Accuracy of Forecasts

by

P.K. Das, N.C. Rai Sircar and D.V. Rao

Contents

Chapter 5.

Prognostic Techniques

In meteorological literature there will be found many methods, empirical or otherwise, for predicting meteorological variables, because that is the ultimate goal of a meteorologist. It is hardly possible in the present monograph to discuss, or even review, all the possible techniques which have been advanced from time to time. Consequently, the main attempt in the present chapter will be to discuss only those methods which appear to be operationally feasible, that is, those which can be completed in the time available at a forecasting centre and with which some experience has been gained in India. An indication of methods on which further experimental work is in progress and the particular difficulties of techniques for low latitudes will be discussed in the next chapter.

Generally, the principal methods followed at present by prognostic units in the different forecasting centres are

(a) prediction on the basis of Rossby waves,

(b) prognosis on the basis of advection of thickness patterns and

(c) Fjortoft's graphical technique for barotropic forecasts.

We may discuss each method separately.

(a) Rossby waves:

A glance at charts depicting mid-latitude contours would readily indicate the presence of a sinusoidal pattern encircling the globe between 30°N and 60°N. The study of waves in a medium like the atmosphere is extremely complicated because the propogation of many different types of wave is possible. It was the genius of Rossby, however, which recognised that by making a few simple assumptions it was possible to filter out all other types of wave motion, except the meteorologically significant ones which we observe on the synoptic chart. The latter are now known as Rossby waves. A very simple relation exists between the speed of propagation of Rossby waves and the wave length of a sinusoidal disturbance. The derivation of this relation will be found in most standard text

books (Petterssen 1956, Haltiner and Martin, 1957) and will not be discussed in detail here. A simple derivation is indicated below to illustrate the main assumptions.

If we assume a non-divergent atmosphere, the conservation of vorticity may be expressed by

$$\frac{d}{dt}(\zeta + f) = 0 \qquad (5.1)$$

The total derivative can be expanded as the sum of a partial derivative and another term to represent the contribution of advection. On neglecting a few other terms whose contributions are generally small, (5.1) may be expressed by

$$\frac{\partial \zeta}{\partial t} + \mathbb{V} \cdot \nabla \zeta + \beta v = 0 \qquad (5.2)$$

where ζ is the vertical component of vorticity, $\mathbb{V}$ is the wind vector and β represents the variation of the coriolis parameter (f) with latitude.

Let us now assume that there was initially a zonal current $(\bar{u})$, on which a disturbance (u,v,w) is subsequently superimposed. Let the perturbations be in the form of waves expressed by

$$u \simeq v \simeq A e^{i\lambda(x - ct)} \qquad (5.3)$$

where λ is the wave number $\left(\frac{2\pi}{L}\right)$, L is the wave length and c is velocity of propagation of the wave. It may be noted from (5.3) that the perturbation is assumed to be independent of the Y-axis, i.e, it is of infinite width in the north-south direction. With these assumptions it readily follows that

$$\zeta = \frac{\partial v}{\partial x} - \frac{\partial u}{\partial y} \simeq i\lambda A e^{i\lambda(x - ct)} \qquad (5.4)$$

whence

$$\frac{\partial \zeta}{\partial t} = \lambda^2 c A e^{i\lambda(x - ct)} \qquad (5.5)$$

The advective term $\mathbf{V}\cdot\nabla\zeta$ in (5.2) is equal to $\bar{u}\frac{\partial \zeta}{\partial x}$, if we neglect the product of small quantities, such as

$$u\frac{\partial \zeta}{\partial x} \quad , \quad v\frac{\partial \zeta}{\partial y}$$

But,

$$\bar{u}\frac{\partial \zeta}{\partial x} \simeq \bar{u}(i\lambda)^2 A e^{i\lambda(x-ct)} \tag{5.6}$$

Hence, if we remove the common factor $Ae^{i\lambda(x-ct)}$, and substitute (5.5) and (5.6) in (5.2) we get

$$\lambda^2 c - \bar{u}\lambda^2 + \beta = 0$$

or, $$c = \bar{u} - \frac{\beta}{\lambda^2}$$

As $\lambda = \frac{2\pi}{L}$, we have

$$c = \bar{u} - \frac{\beta L^2}{4\pi^2} \tag{5.7}$$

which is Rossby's formula.

When the wave is stationary $(c = 0)$,

$$\bar{u} = \frac{\beta L^2}{4\pi^2} \tag{5.8}$$

If we indicate the wave length of the stationary wave by L_s, we may express (5.7) as by

$$c = \frac{\beta}{4\pi^2}(L_s^2 - L^2) \tag{5.9}$$

With the help of (5.8), the stationary wave length can be computed for different zonal wind speeds ($\bar{u}$) and for different latitude circles (β = constant). On dividing the circumference of each latitude circle by the stationary wave length, we obtain the stationary hemispherical wave number. A few typical values for three latitudes are given in Table I.

TABLE - I

Values of the stationary wave length

Latitude	Element	$\bar{u}$ (m/sec) 4	15	20
60	L_s in deg. Long.	66	115	149
	Stationary wave No.	5	3	2
45	L_s in deg. Long.	40	69	89
	Stationary wave No.	9	5	4
30	L_s in deg. Lang.	29	51	66
	Stationary wave No.	12	7	5

As seen from the above table, the stationary wavelength decreases and the stationary wave number increases rapidly with decreasing zonal wind speed. The actual number of Rossby waves seldom differs by more than one from the stationary wave number. Once established, stationary long waves persist for several days. Short wave troughs intensify as they approach stationary wave troughs and weaken as they move towards stationary wave ridges.

Rossby's formula has been modified by Petterssen (1956) to include the finite width of the zonal current and the tilt of the wave. Petterssen's formula is

$$C = \frac{\left(\bar{u} - \frac{\beta L^2}{4\pi^2}\cos\gamma\right)}{\left[1 + \left(\frac{L}{2\pi B}\right)^2\right]} \qquad (5.10)$$

where γ is the tilt of the wave (angular deviation of the trough or ridge line from the meridian) and B is the half-width of the zonal current. The half-width is the distance from the axis of the current at which wind speed drops to half its maximum value. In general, it is simpler to use Rossby's original formula but, for greater refinement, Petterssen's formula is useful.

Experiments with Rossby's equation, or the modified equation of Petterssen have revealed a fair degree of success for wave patterns which move across China and Tibet north of the Himalayan barrier. In regions south of 30 N, there is evidence of another system of transient troughs, which are often referred to as 'waves in the easterlies'. Rossby's equation has not been found to be very successful for predicting the displacement of these troughs. This is mainly because the (i) zonal current ($\bar{u}$) is generally weak and (ii) the wavelength is small compared to that of extra-tropical disturbances. Added to this is the difficulty of fixing the position of troughs and ridges in a region of inadequate coverage of upper wind data.

(b) Adevection of thickness patterns:

This method consists in preparing the following charts:

i) Surface prognostic (Pressure),
ii) 1000 mb prognostic,
iii) 1000-500 mb prognostic thickness,
iv) 500 mb prognostic,
v) 500-300 mb prognostic thickness,
vi) 300 mb prognostic,
vii) 300-200 mb prognostic thickness and
viii) 200 mb prognostic.

The preparation of each chart is discussed below:

i) Surface prognostic chart.

The pressure change for the next twenty four hours, at numerous selected stations over the area in which we are interested, are estimated from the pressure change and departure charts of the day and also of the preceding few days. In this connection, the movements of the surface pressure system is also carefully watched. The success of prognosis for upper air charts largely depends on the accuracy with which forecasts are made of the pressure change. The estimated pressure changes are added to the current pressure values and the forecast

pressures thus obtained are plotted on a separate chart. The isobars are next drawn to complete the prognosis. In this way the surface prognostic chart for 0000 GMT of the next day is obtained from the 0000 GMT current data. Temperature forecasts for different stations are also made in the same way from the temperature changes and departures from normal for the past 72 hours. The forecast temperaturesare then plotted on the surface prognostic chart.

(ii) 1000 mb prognostic chart.

The height of the 1000 mb surface over different stations is determined from the pressure and temperature data on the surface prognostic chart with the help of a table and plotted on a separate chart. Isopleths are then drawn at intervals of 20 gpm. The pattern thus obtained represents the 1000 mb prognostic chart.

(iii) 1000-500 mb prognostic thickness chart.

Current thickness values of the 1000-500 mb layers over all available Radiosonde stations in the region are plotted. Shear winds between 0.6 km and 5.8 km for all available Rawin and Pilot Balloon stations are also plotted on the same chart in red-ink, following the usual convention of plotting of shear winds. Thickness lines are then drawn at intervals of 20/40 gpm giving greater weightage to wind shear wherever the thickness values do not fit properly. It has been found from experience that the thickness patterns are more conservative than the contour patterns. Their day-to-day changes are usually small and more systematic. To estimate the direction of movement of thermal troughs and ridges, the winds at 3 km (the mean level) are also plotted on the above charts. From these charts the prognostic thickness pattern is constructed, keeping in view the requirement of continuity with the previous day's pattern.

(iv) 500 mb prognostic chart.

The prognostic thickness chart is placed over the 1000 mb prognostic chart on a light table, and the points of intersection are marked. Contour lines are then drawn connecting the intersection points at intervals of 40 gpm.

Upper air temperatures are also forecast on the assumption that the changes are mainly caused by advection. The thickness chart is found useful for this purpose. Forecast temperatures for selected stations are plotted on the 500 mb prognostic chart and isotherms are drawn.

(v) 300 and 200 mb prognostic chart.

The procedure for the construction of these charts is a repetition of the method employed for the preparation of the 500 mb prognostic chart. Prognostic thickness patterns between 500 and 300 mb and between 300-200 mb are prepared and superposed on 500 and 300 mb prognostic charts to obtain the prognostic charts for 300 and 200 mb

The prognostic charts prepared by this method were compared with the corresponding actual charts to make a qualitative assessment of the accuracy. It was found that if a verification was made by strictly comparing the actual geopotential heights with forecast values at selected points then the performance was not very encouraging. On the other hand, if a verification was made by way of qualitative agreement, that is, by examining whenever the forecast wind and temperature data satisfy the tolerance permitted for aviation forecasts, then the performance was much more satisfactory. In preparing prognostic charts by this method, the experience and skill of the forecaster admittedly plays an important role.

(c) Fjortoft's graphical technique:

(i) Theoretical basis.

Fjortoft has described a simple method for constructing 500 mb prognostic charts by graphical integration of the vorticity equation. For full details of

the method a reference may be made to Fjortoft's original paper (Fjortoft, 1952). In this note, we shall be mainly concerned with the practical aspects of the technique with the objective of introducing short-cuts wherever possible.

If we assume a barotropic and non-divergent atmosphere, then the conservation of vorticity may be expressed by the equation

$$\frac{\partial \zeta}{\partial t} + \mathbf{V} \cdot \nabla (\zeta + f) = 0 \qquad (5.11)$$

where ζ is the vertical component of vorticity, f is the coriolis parameter and $\mathbf{V}$ is the wind vector. Now, for geostrophic motion we may also express the zonal and meridional velocity components (u,v) by

$$u = -\frac{g}{f}\frac{\partial z}{\partial y} \quad ,$$

$$v = \frac{g}{f}\frac{\partial z}{\partial x} \qquad (5.12)$$

where g is the acceleration due to gravity and z is the height of a pressure surface. The derivation of (5.12) is straightforward and may be found in standard text books (Petterssen, 1956, Haltiner and Martin, 1957). The advantage of using the geostrophic relation is that it yields a simple relation between the topography of a constant pressure surface (Z) and the vorticity (ζ). Thus, on using (5.12) we have

$$\zeta = \frac{\partial v}{\partial x} - \frac{\partial u}{\partial y} = \frac{g}{f}\nabla^2 z \qquad (5.13)$$

where

$$\nabla^2 = \frac{\partial^2}{\partial x^2} + \frac{\partial^2}{\partial y^2} \qquad (5.14)$$

From the contour pattern on a constant pressure chart we may readily obtain the field of Z. From this field it is a fairly simple operation to compute $\nabla^2 z$ i.e., the vorticity, by using finite differences in place of derivatives.

Let us divide the region under consideration into a series of small squares, as shown in Figure 1. Our aim is to find the vorticity (ζ) at the centre of each unit grid, where the height of the isobaric surface is, say, Z_o. Referring to Figure 1, we can see that

$$\frac{\partial^2 Z}{\partial x^2} = \frac{1}{H}\left[\frac{z_1 - z_0}{H} - \frac{z_0 - z_3}{H}\right] = \frac{z_1 + z_3 - 2z_0}{H^2}$$

$$\frac{\partial^2 z}{\partial y^2} = \frac{z_2 + z_4 - 2z_0}{H^2} \qquad (5.15)$$

whence

$$\zeta = \frac{g}{fH^2}\left[\left(z_1 + z_2 + z_3 + z_4\right) - 4z_0\right] \qquad (5.16)$$

Putting

$$4\bar{Z} = z_1 + z_2 + z_3 + z_4$$

We get

$$\zeta = \frac{4g}{fH^2}\left(\bar{Z} - z_0\right) \qquad (5.17)$$

The physical picture behind the above algebraic operations is simple. What we have done is to introduce a hypothetical field ($\bar{Z}$) by averaging the values of Z at the four corners of each square. The vorticity is then expressed by a simple relation between $\bar{Z}$ and Z_0 at the centre of each square by equation (5.17).

At this stage we have to note that, in graphical integration, one has to deal with actual measurements that appear on a chart and convert them into values representative of the atmosphere. A synoptic chart is essentially a mapping of lines on a sphere into lines on a two-dimensional plane. The maps used in meteorology are generally 'conformal', i.e., the angle between two intersecting lines on the original sphere is preserved by the transformation. This property is generally achieved by introducing a certain amount of distortion of the lines, so that if H is the distance between two points on the map, the actual distance (H') on the earth's surface will be

$$H = \frac{H}{m} \tag{5.18}$$

where m is the map factor. The map factor is a function of latitude but, in general, its variation is small, so that we can usually regard it as a constant. Noting (5.18), we can see that the vorticity given by (5.17) has to be multiplied by m^2 to make it representative of the atmosphere. Thus,

$$\zeta = \frac{4m^2 g}{fH^2} (\bar{z} - z) \tag{5.19}$$

We can now substitute (5.19) into (5.11) to derive an expression for the vorticity equation in terms of Z and $\bar{Z}$ alone. We have

$$-\frac{\partial}{\partial t}(z - \bar{z}) = \mathbf{V} \cdot \nabla (z - \bar{z}) - \frac{fH^2}{4m^2 g} \mathbf{V} \cdot \nabla f \tag{5.20}$$

Noting that

$$f = 2\Omega \sin\phi$$

where Ω is the speed of angular rotation of the earth and ϕ is the latitude, we see that

$$\begin{aligned}
\frac{fH^2}{4m^2 g} \mathbf{V} \cdot \nabla f &= \left(\frac{H^2}{4m^2 g}\right)\left(2\Omega \sin\phi\right) \mathbf{V} \cdot \left(2\Omega \cos\phi \, d\phi\right) \\
&= \left(\frac{H^2}{4m^2 g}\right) \frac{(2\Omega \sin\phi)^2}{\sin\phi} \mathbf{V} \cdot (\cos\phi \, d\phi) \\
&= \mathbf{V} \cdot \left(\frac{f^2 H^2}{4m^2 g}\right) (\cot\phi \, d\phi)
\end{aligned}$$

Putting

$$\int_0^{\phi} \frac{f^2 H^2}{4m^2 g} \cot\phi \, d\phi = G$$

we get

$$\frac{fH^2}{4m^2 g} \mathbf{V} \cdot \nabla f = \mathbf{V} \cdot \frac{f^2 H^2}{4m^2 g} \cot\phi \, d\phi = \mathbf{V} \cdot \nabla G \tag{5.21}$$

Substitution of (5.21) in (5.20) yields

$$\frac{\partial}{\partial t}(z - \bar{z}) = -\mathbf{V} \cdot \nabla (z - \bar{z} - G) \tag{5.22}$$

Equation (5.22) could be integrated directly, if we use very small time increments in which $\mathbb{V}$ is reasonably steady. Unfortunately, the labour involved would be prohibitive, because the wind vector ($\mathbb{V}$) is a very variable quantity. Fjortoft showed that this irksome hurdle could be overcome if we introduce a hypothetical wind ($\overline{\mathbb{V}}$), measured by the gradient of $\bar{Z}$, which is substantially more steady than $\mathbb{V}$. Consequently, the integration could be performed in just one time step of 24 hours. To see how this can be done let us put

$$Z = (\bar{Z} + G) + (z - \bar{Z} - G)$$

whence

$$\nabla Z = \nabla (\bar{Z} + G) + \nabla (z - \bar{Z} - G) \tag{5.23}$$

For geostrophic motion we can express (5.12) in the vectorial form

$$\mathbb{V} = -\frac{g}{f} \nabla Z \times \mathbb{k} \tag{5.24}$$

where $\mathbb{k}$ is the unit vector along the vertical. Substitution of (5.23) in (5.24) gives

$$\mathbb{V} = -\frac{g}{f} \left[\nabla (\bar{Z} + G) \times \mathbb{k} + \nabla (z - \bar{Z} - G) \times \mathbb{k} \right] \tag{5.25}$$

With this expression for $\mathbb{V}$ we are now in a position to evaluate the advective term on the right hand side of (5.22). We have

$$\begin{aligned} \mathbb{V} \cdot \nabla (z - \bar{Z} - G) = & -\left[\frac{g}{f} \nabla (\bar{Z} + G) \times \mathbb{k} \right] \cdot \nabla (z - \bar{Z} - G) \\ & - \left[\frac{g}{f} \nabla (z - \bar{Z} - G) \times \mathbb{k} \right] \cdot \nabla (z - \bar{Z} - G) \end{aligned} \tag{5.26}$$

The second dot product on the right hand side of (5.26) vanishes because $\nabla (z - \bar{Z} - G) \times \mathbb{k}$ is a vector perpendicular to $\nabla (z - \bar{Z} - G)$ and $\mathbb{k}$. Consequently, its dot product with $\nabla (z - \bar{Z} - G)$ must vanish. We are thus left with

$$\mathbb{V} \cdot \nabla (z - \bar{Z} - G) = -\left[\frac{g}{f} \nabla (\bar{Z} + G) \times \mathbb{k} \right] \cdot \nabla (z - \bar{Z} - G)$$

In agreement with the geostrophic relation, (5.24) let us define two hypothetical winds ($\overline{\mathbb{V}}$) and C defined by the gradients of $\bar{Z}$ and G. Thus

$$\overline{\mathbb{V}} = -\frac{g}{f} \nabla \bar{z} \times \mathbb{k}$$

$$C = -\frac{g}{f} \nabla G \times \mathbb{k} \qquad (5.27)$$

Substitution of the above in (5.26) and (5.22) gives

$$\frac{\partial}{\partial t} (z - \bar{z}) = -(\overline{\mathbb{V}} + C) \cdot \nabla (z - \bar{z} - G) \qquad (5.28)$$

We have thus achieved what we had set out to do, namely, to show how the fluctuating $\mathbb{V}$ can be replaced by $(\overline{\mathbb{V}} + C)$ which is a hypothetical wind for advecting the field of $(z - \bar{z} - G)$. The right hand side of (5.28) is sometimes expressed exclusively in terms of Z, $\bar{Z}$ and G. To do this let $\bar{u}, \bar{v}, C_x, C_y$ represent the zonal and meridional components of $\overline{\mathbb{V}}$ and C. From (5.27) we have

$$\bar{u} = -\frac{g}{f} \frac{\partial \bar{z}}{\partial y} \quad ; \quad \bar{v} = \frac{g}{f} \frac{\partial \bar{z}}{\partial x} \quad ,$$

$$C_x = -\frac{g}{f} \frac{\partial G}{\partial y} \quad ; \quad C_y = \frac{g}{f} \frac{\partial G}{\partial x}$$

whence,

$$\bar{u} + C_x = \frac{-g}{f} \frac{\partial}{\partial y} (\bar{z} + G) \quad , \quad \bar{v} + C_y = \frac{g}{f} \frac{\partial}{\partial x} (\bar{z} + G)$$

But,

$$(\overline{\mathbb{V}} + C) \cdot \nabla (z - \bar{z} - G) = (\bar{u} + C_x) \frac{\partial}{\partial x} (z - \bar{z} - G) + (\bar{v} + C_y) \frac{\partial}{\partial y} (z - \bar{z} - G)$$

$$= \frac{g}{f} \left[-\frac{\partial}{\partial y} (\bar{z} + G) \frac{\partial}{\partial x} (z - \bar{z} - G) \right.$$

$$\left. + \frac{\partial}{\partial x} (\bar{z} + G) \frac{\partial}{\partial y} (z - \bar{z} - G) \right] \qquad (5.29)$$

The right hand side of the above equation may be identified as a Jacobian operator (J). If α, β be two functions of x and y then

$$J(\alpha, \beta) = \frac{\partial \alpha}{\partial x} \frac{\partial \beta}{\partial y} - \frac{\partial \alpha}{\partial y} \frac{\partial \beta}{\partial x}$$

whence it follows from (5.28) and (5.29) that

$$\frac{\partial}{\partial t} (z - \bar{z}) = -\frac{g}{f} J (\bar{z} + G, z - \bar{z} - G) \qquad (5.30)$$

There is no basic difference between (5.28) and (5.30). The only important physical concept that has to be remembered is the necessity of replacing V by the more conservative wind ($\overline{V} + C$) in (5.28).

Suppose we now use a time step (Δt) of 24 hours. The new Z field at the end of 24 hours will be given by

$$Z_{t+24} = Z_t + \left(\frac{\partial z}{\partial t}\right) \Delta t \qquad (5.31)$$

from (5.30) we know that

$$\frac{\partial Z}{\partial t} = \frac{\partial \overline{z}}{\partial t} - \frac{g}{f} J\left(\overline{z} + G\ ,\ z - \overline{z} - G\right) \qquad (5.32)$$

Substitution of (5.32) in (5.31) would give us the new Z field, if we knew the new values of $\overline{Z}$ and $J(\overline{z}+G\ ,\ z-\overline{z}-G)$.

The way to do this is to put

$$\frac{g}{f}\left\{J(\overline{z}+G)\ ,\ z-\overline{z}-G)\right\}\Delta t = \delta(z-\overline{z}-G) = P \quad \text{(say)}$$

$$\frac{\partial \overline{z}}{\partial t} \times \Delta t = \delta \overline{z} \qquad \text{and}$$

$$Z_{t+24} - Z_t = \delta Z$$

We have from (5.30)

$$\delta Z = \delta \overline{z} - P$$

The space average of this equation is

$$\delta \overline{z} = \delta \overline{\overline{z}} - \overline{P}$$

Elimination of $\delta \overline{z}$ yields,

$$\delta z = -P - \overline{P} + \delta \overline{\overline{z}}$$

If the process of averaging is continued n times,

we get

$$\delta Z = -P - \overline{P} - \overline{\overline{P}} + \cdots\cdots\cdots\cdots + \delta \overline{z}^{(n+1)}$$

Fjortoft showed that a more rapidly converging series may be obtained by increasing the distance for the successive space averages. Using this technique he derived the following formula for computing height changes,

$$\delta z = -P - 2\bar{P} - 4\bar{\bar{P}} \cdots\cdots$$

In general, it is sufficient to use either the first term or only the first two terms, viz.,

$$\delta z \simeq -P - 2\bar{P} \qquad (5.33)$$

Equation (5.33) gives the complete equation for prediction by Fjortoft's method. At some forecasting centres in India, the complete prediction equation is somewhat simplified, by the use of short-cuts. In the following sections we shall consider a few methods of shortening the process.

Let us first consider (5.28)

$$\frac{\partial}{\partial t}(z-\bar{z}) = -(\bar{V}+C)\cdot\nabla(z-\bar{z}-G)$$

In general, C and G are small compared to $\bar{V}$ and $\bar{z}$. Consequently, we may put

$$(\bar{V}+C)\cdot\nabla(\bar{z}+G) = 0$$

because this is largely the dot product of $\bar{V}$ and $\nabla\bar{z}$, i.e., the dot product of two perpendicular vectors. Hence, for practical purposes(5.28) may be written as

$$\frac{\partial}{\partial t}(z-\bar{z}) = -(\bar{V}+C)\cdot\nabla z \qquad (5.34)$$

At this stage it is possible to introduce a further short cut. Let us assume that the field of $\bar{z}$ remains reasonably steady in 24 hours, i.e, its variation are small compared to variation of z. This implies that

$$\frac{\partial\bar{z}}{\partial t} = 0$$

so that we have

$$z_{t+24} = z_t - \left[(\bar{V}+C)\cdot\nabla z\right]\Delta t \qquad (5.35)$$

The use of (5.35) is equivalent to using only the first term of the series (5.33). Experiments conducted at a few forecasting centres indicate that there is often no substantial loss of accuracy if we use (5.35) instead of (5.33). Admittedly, it implies a little sacrifice in mathematical accuracy,

but its justification lies in the saving of time and manpower.

(ii) Choice of the grid interval (H).

Delineation of long wave troughs and ridges by smoothening out the short waves is achieved by choosing an appropriate distance (H) for the unit grid, because the field of G essentially reflects the influence of the earth's rotation and, in graphical procedure, this is weighted by H^2. A grid interval (H) of 600 km was found by Fjortoft to be capable of yielding a 24 hour forecas in one time step. But, Estoque (1955) found better agreement between observed and predicted values of Z with a grid interval of 1000 km. Opinion is a little divided on the appropriate value of the grid interval, but it is instructive to examine the effect of this parameter on the overall accuracy of the method.

Fjortoft advocated a large value of H because, in the averaing process for $\bar{Z}$, this helped to damp out short and medium scale waves. We may illustrate his argument by the following simple case.

Consider the following sinusoidal contour pattern

$$Z = A \sin \frac{2\pi x}{\lambda} \sin \frac{2\pi y}{\eta} \qquad (5.36)$$

Let us see what is the effect of constructing $\bar{Z}$ from the above field of Z. We have

$$\bar{Z} = \frac{1}{4}\left[Z_{x+H} + Z_{x-H} + Z_{y+H} + Z_{y-H} \right]$$

But,

$$Z_{x+H} = A \sin\frac{2\pi}{\lambda}(x+H) \sin \frac{2\pi}{\eta} y$$

$$= A\left(\sin\frac{2\pi x}{\lambda} \cos \frac{2\pi H}{\lambda} + \cos\frac{2\pi x}{\lambda} \sin \frac{2\pi H}{\lambda}\right) \sin \frac{2\pi y}{\eta}$$

Similar expressions may be obtained for Z_{x-H}, Z_{y+H} ..... etc. If we add all such expressions we eventually get

$$\bar{Z} = Z \times \frac{1}{2}\left(\cos \frac{4\pi H}{\lambda} + \cos \frac{4\pi H}{\eta}\right) = DZ \qquad (5.37)$$

We can thus see that the effect of constructing Z out of Z is to reduce the amplitude of the original Z field by a damping factor D.

Let us assume for simplicity $\lambda = \eta$. The two cases of interest are:-

(a) $\frac{H}{\lambda} = \sum_{1}^{\infty} \frac{n}{4}$ i.e. $H = \frac{\lambda}{4}, \frac{2\lambda}{4}$, etc.

whence

$$D = \cos n\pi = 1$$

This implies no damping of the original Z field

(b) $$\frac{H}{\lambda} = \sum_{1}^{\infty} \frac{2n-1}{8}$$

When $D = 0$,

which implies complete damping of the Z field.

Thus, it is preferable to choose H as some multiple of $\frac{\lambda}{8}$. Suppose we choose $H = \frac{\lambda}{8}$ and examine the behaviour of the damping factor (D) for different wave lengths. A few calculations on the basis of (5.37) yields the values shown in Table II.

TABLE - II

Variation of D for different values of λ

λ	8H	10H	12H	16H	24H
D	0	.3	.5	.7	.9

The figures illustrate how short waves tend to get damped out, while the longer ones are left comparatively undisturbed.

Despite the above advantage of using a large H, there is yet another aspect which merits consideration. It will be noted that we have replaced the vorticity ($\nabla^2 Z$) by its equivalent in finite-differences $\frac{4}{H^2}(\bar{Z} - Z)$.

How good is this approximation?

We can estimate the error by expanding Z(X+ H) and Z(X - H) in a Taylor series about the central point X,Y. Thus

$$Z(X+H) = Z_{xy} + HZ' + \frac{H^2}{2!} Z'' + \frac{H^3}{3!} Z''' + \frac{H^4}{4!} Z^{IV} + \cdots\cdots$$

$$Z(X-H) = Z_{xy} - HZ' + \frac{H^2}{2!} Z'' - \frac{H^3}{3!} Z''' + \frac{H^4}{4!} Z^{IV} - \cdots\cdots$$

On addition

$$\frac{1}{H^2}\left[Z(X+H) + Z(X-H) - 2Z(XY)\right] = \frac{\partial^2 Z}{\partial x^2} + \frac{H^2}{12} Z^{IV}$$

The last term on the right hand side indicated that the order of magnitude of the error is proportional to H^2. Thus, if we were to double the value of H, the error would be increased four times.

We may thus conclude that although a large value of H helps to damp out short waves, it gives a poor representation of the vorticity. For this reason a smaller H, of the order of 464 km is sometimes used as a compromise.

(iii) Calculation of G (ϕ).

G represents the approximate contribution of the earth's rotation to the absolute vorticity. Contours of G are determined only by f and m, which depend on the latitude. As long as the same map projection is used, the G field would remain the same and can be constructed once for all. A few typical values for H = 464 km are shown in Table III. In figure 2 we have also shown values of G computed for a larger grid interval (H = 1000 km).

TABLE - III

Values of G for different latitudes

Latitude	G (metres)	Latitude	G (metres)
10	2.5	40	52.5
20	15.0	50	75.0
30	30.0	60	96.5

Thus we can see that $\vec{C}$, which is measured by the gradient of G, is a vector directed from the east to west. Its sense is, therefore, opposed to $\overrightarrow{\nabla V}$ for regions north of 30°N. The magnitude of C, as computed from values in Table III, is approximately 5 knots north of 45°N and negligibly small south of 45°N.

(iv) Practical steps for routine preparation of prognostic charts.

Step I : Preparation of $\bar{Z}$, $\bar{Z} - Z$ chart.

The $(\bar{Z} - Z)$ field represents the Laplacian of Z and is proportional to the geostrophic relative vorticity. Positive values of $(\bar{Z} - Z)$ correspond to cyclonic vorticity, while negative values represent anticyclonic vorticity. Transient short wave troughs (ridges) thus appear as moving centres of positive (negative) $(\bar{Z} - Z)$ isopleths. The $\bar{Z}$ and $(\bar{Z} - Z)$ fields together portray graphically the horizontal advection of vorticity. The construction of the $\bar{Z}$, $\bar{Z} - Z$ charts is carried out in the following steps.

i) We make two copies of A and B of the 500 mb chart. For reference purposes, a large cross may be put at two convenient points on the two charts. Place B on top of A and see that the crosses coincide. On a light table, place a blank map, C, over A and B. Place two crosses on C at the same place as on A and B. The crosses on all three maps should now be exactly at the same spot, indicating that the maps are flush on top of one another in the order A, B and C starting from the bottom.

ii) Hold B and C steady and displace A a distance $H/\sqrt{2}$ (.707H) to the north. The crosses on A should now be $H/\sqrt{2}$ to the north of those on B and C. Fix the positic of A with adhesive tape. Hold C steady and displace B a distance $H/\sqrt{2}$ to the south. Fix the position of B with either adhesive tape or pin. If the operations are done correctly, the crosses on A and B should now be separated by a distance $2H/\sqrt{2}$, while the map C should be centred betwee..

the two, that is, it should be at a distance $H/\sqrt{2}$ relative to A and B.

iii) Add the analysis of A and B graphically on C connecting every other set of intersections. The purpose of this operation is to construct the isopleths of $\frac{1}{2}(Z_2 + Z_4)$. Z_2, Z_4 are points on the square grid shown in figure 1.

iv) Trace the analysis on map C on another map D.

v) Displace map C a distance $2H/\sqrt{2}$ to the right or left of map D. On a light table place yet another blank map E over both C and D, such that E is centred between C and D. The procedure for displacing C a distance of $2H/\sqrt{2}$ to the right (or left) with respect to D, and having E centred between the two is exactly the same as explained above.

vi) On map E, average graphically the analysis from C and D. The result is the $\overline{Z}$ field. Note that in preparing $\overline{Z}$ we do not get any intersection points within a distance $2H/\sqrt{2}$ from the edge of the map.

vii) Superimpose chart E on the 500 mb contour (Z) chart and substract graphically on another blank map connecting all sets of intersections. This gives us the $(\overline{Z} - Z)$ charts(F chart).

Admittedly the above operations use up a large number of blank maps. This may be overcome by the use of "Acetate" transparencies or thin tracing paper. The operations are not difficult and after a little practice can be completed quite rapidly.

Step 2: $(\overline{Z} + G)$ or the advecting vorticity field.

Superimpose the $\overline{Z}$ chart on the G field and add graphically. This gives us chart P.

Step 3: $(Z - \overline{Z} - G)$ or the advected field.

To get this we substract graphically the $(\overline{Z} + G)$ field from the Z field. The resulting chart may be called Q.

Step 4 : Prognostic $(Z - \bar{Z} - G)$ or the prognostic advected field.

Superimpose the $(\bar{Z} + G)$ chart (P) on the $(Z - \bar{Z} - G)$ chart (Q). Advect the $(Z - \bar{Z} - G)$ field along the $(\bar{Z} + G)$ contours by the average geostrophic wind along the entire trajectory during the prognostic period of 12 or 24 hours. This gives the prognostic vorticity field, say, chart R.

Step 5 : The 500 mb prognostic chart.

Add graphically the $(\bar{Z} + G)$ field (Chart P) to the $(Z - \bar{Z} - G)$ prognostic field (Chart R). This gives the prognostic 500 mb chart (Chart S). The simplification involved in this step is equivalent to considering only the first term in the series (5.33). Experience shows that from the practical point of view this is generally satisfactory.

In order to distinguish the lines on the different charts during the graphical operations, it is desirable to adopt a suitable colour scheme, such as the following:

1. A (500 mb contours)	: Black
2. B (duplicate 500 mb)	: Blue
3. C	: Red
4. D	: Black
5. E ($\bar{Z}$ field)	: Black
6. F ($\bar{Z} - Z$ field)	: Purple
7. P ($\bar{Z} + G$ field)	: Green
8. Q ($Z-\bar{Z}-G$ field)	: Red
9. R (Prognostic $Z-\bar{Z}-G$)	: Black
10. S (500 mb prognostic)	: Purple

In figures 3,4,5 and 6 we have reproduced charts to illustrate the type of result we may expect from this method.

The charts are for :

a) 500 mb Z field for a typical situation on 15.1.1963,

b) $\bar{Z}$ field for the same chart,

c) $Z-\bar{Z}-G$ field and

d) the prognostic and actual 500 mb chart for 16.1.63.

It is appropriate to indicate here that if we had used the abbreviated technique indicated by equations (5.34) and (5.35), the procedure to be followed after the preparation of the Z field would be slightly different. The differer steps in this case are given below:-

Step 2'

Take the original Z field for 500 mb and mark out all trough lines, axes of ridges and other points of interest. From the isopleths of $\bar{Z}$ compute the mean value of $\overline{|V|}$ (which is only the geostrophic wind corresponding to isopleths of $\bar{Z}$) at or near the axes of troughs, ridges etc.

Step 3' :

Displace the axes of troughs or ridges in the direction of $\overline{|V|}$ by the distance likely to be covered in the forecast interval (24 hours), if the average speed of movement was ($\overline{|V|} + C$). As mentioned earlier, a speed of 5 knots has to be deducted from $\overline{|V|}$ for regions north of 45°N. For regions south of 45°N no correction is necessary. It is useful to construct a nomogram to deduce the displacement in 24 hours for different speeds.

Step 4' :

After the axes of trough/ridges have been displaced the new Z field can be drawn in keeping the same symmetry as the original 500 mb map. This gives us the prognostic 500 mb map.

The barotropic model enables us to derive the prognostic 500 mb chart by gr: phical methods. The model assumes a non-divergent atmosphere and geostrophic wi: flow. But the thermodynamic processes and the conditions of flow at the upper

and lower boundaries of the earth's atmosphere, such as, the influence of the topography of the earth's surface and non-adiabatic heat flow are not taken into account in this model.

We have to also note that the barotropic forecast of the 500 mb chart cannot indicate developments, such as, the intensification or weakening of pressure systems. To infer the development we have to rely on past history, the delineation of the thermal field and other factors. This aspect of the problem will be discussed in the next chapter.

REFERENCES

1. Estoque, M.A. 1955 : Univ. of Chicago, Dept. Met., Tech. Rept. 5.
2. Fjortoft, R. 1952 : Tellus, Stockholm, 4,3.
3. Haltiner, G.J. and Martin, F.L. 1957: Dynamical and Physical Meteorology, McGraw Hill Book Co., New York.
4. Petterssen, S. 1956: Weather Analysis and Forecasting, McGraw Hill, New York.
5. Saucier, W.J. 1959: Principles of Meteorological Analysis. Univ. of Chicago Press, Second Impression.
6. World Meteorological Organization. 1961: Techniques for High-Level analysis and forecasting of wind and temperature fields. Tech. Note No. 35, Geneva.

Chapter 6

Future extensions of prognostic techniques

In this chapter we will discuss a few methods with which preliminary experiments are in progress. The methods are primarily aimed at (a) the inclusion of baroclinic effects in prognosis and (b) a modification of Fjortoft's method by the inclusion of climatic normals instead of the $\bar{Z}$ field. In the concluding parts of the chapter we also consider a few techniques suitable for low latitudes

6.2 Graphical techniques for inclusion of baroclinic effects.

While discussing Fjortoft's technique we pointed out two main limitations of the barotropic model, namely, (a) it permits no weakening or intensification of pressure systems and (b) the direction of the wind vector is assumed to be independent of height. A number of models have been constructed (Eady, 1952, Charney and Phillips, 1953, Sawyer and Bushby, 1953, Estoque, 1955 and Eliassen, 1956) to overcome these limitations, but it is not very clear whether these models are vastly superior to the simpler barotropic model. Generally, there is little difference between the several baroclinic models which have been constructed. As the ultimate selection is largely a matter of choice, the present note will be concerned with Eliassen's model (1956), which is in many ways convenient for graphical integration.

6.2.1 Physical basis of the model.

We can generally resolve a vector quantity, such as the wind, into two parts, i.e., one which has no divergence and another which exhibits no rotation (vorticity). These two components of the wind may be denoted by the superscripts 'nd' and 'ir'. Thus,

$$\mathbf{V}(x, y, p, t) = \mathbf{V}^{nd} + \mathbf{V}^{ir} \qquad (6.2.1.1)$$

Let us first consider the non-divergent part. We may assume that this is the vector sum of a mean wind ($\mathbf{V}_m$) and a thermal wind ($\mathbf{V}_T$) multiplied by an arbitrary co-efficient $\beta(p)$. Hence,

$$\mathbb{V}^{nd} = \mathbb{V}_m + \beta(p)\,\mathbb{V}_T \qquad (6.2.1.2)$$

$\mathbb{V}_m$ refers to the wind at the mean level of the atmosphere and the coefficient $\beta(p)$ is a function of pressure. For convenience in notation, the superscript (nd) may be henceforth dropped. We may proceed on the understanding that we are dealing with the non-divergent part, until the irrotational component is specifically mentioned.

In agreement with (6.2.1.2), it follows that the vorticity at any level may be expressed as the vector sum of a mean vorticity and a thermal vorticity multiplied by $\beta(p)$. We have

$$\zeta(x, y, p, t) = \zeta_m + \beta(p)\,\zeta_T \ . \qquad (6.2.1.3)$$

As we can see from the above equations, if the direction of $\mathbb{V}_m$ and $\mathbb{V}_T$ is the same, then

$$\mathbb{V} = \left[\mathbb{V}_m\,(1 + \beta\,\mathbb{V}_T/\mathbb{V}_m)\right] \simeq A\,\mathbb{V}_m \quad \text{(say)},$$

where

$$\beta = (A-1)\,\mathbb{V}_m / \mathbb{V}_T$$

The above represents the equivalent barotropic model; so that the baroclinic model reduces to the equivalent barotropic model if $\mathbb{V}_m$ and $\mathbb{V}_T$ are in the same direction.

There is another important physical constraint in the baroclinic model. The above equations (6.2.1.2 and 6.2.1.3) reveal that the direction of the wind shear remains invariant in a given column of the atmosphere. From (6.2.1.2) we can see that

$$\frac{\partial \mathbb{V}}{\partial p} = \frac{\partial \beta}{\partial p}\,\mathbb{V}_T$$

As $\beta(p)$ is a scalar quantity, it follows that the direction of the wind shear cannot change. This is illustrated in figure 7. Suppose the wind vector at

900, 800, 700 ..... mb was represented by V_9 , V_8 , V_7 etc., then the shear vector would trace out the straight line ABCD.

The above representation of the wind and vorticity can now be used in the simplified vorticity equation

$$\frac{\partial \zeta}{\partial t} = -V \cdot \nabla (\zeta + f) + f \frac{\partial \omega}{\partial p}$$

Substitution of (6.2.1.2) and (6.2.1.3) in the above equation yields

$$\frac{\partial}{\partial t}(\zeta_m + \beta \zeta_T) = -(V_m + \beta V_T) \cdot \nabla (\zeta_m + \beta \zeta_T + f) + f \frac{\partial \omega}{\partial p} \quad (6.2.1.4$$

Let us now take the average of the above equation with respect to the atmosphere. This implies finding the integral

$$\frac{1}{\partial p} \int_{p_o}^{o} (\quad) \, dp$$

for each term of (6.2.1.4). Noting that

$$\beta_m = 0$$

we get

$$\frac{\partial \zeta_m}{\partial t} = -V_m \cdot \nabla (\zeta_m + f) - (\beta^2)_m V_T \cdot \nabla \zeta_T + f \frac{\omega_G}{p_G} \quad (6.2.1.$$

where the subscript 'G' refers to values at the ground. For simplicity, let us assume that $\omega_G = 0$ This will not be a valid assumption for mountainous terrain, but for the present we shall retain this assumption. With this assumption, we get

$$\frac{d}{dt}(\zeta_m + f) = -(\beta^2)_m V_T \cdot \nabla \zeta_T \quad (6.2.1.$$

Equation (6.2.1.5) expresses the main difference between a barotropic and a baroclinic model. While a barotropic model conserves the absolute vorticity at the mean level (m), the baroclinic model permits a change in the absolute vorticity. This change is brought about by advection of the thermal vorticity by the thermal wind. We can see how this operates in practice by referring to a few common synoptic situations.

Let us first consider the case when contour lines and isotherms (lines of equal thickness) are in phase at all levels. This is shown in figure 8. Referring to (6.2.1.5), we see that both the advective terms on the right hand side have the same sign. Consequently, the thermal field reinforces the advection of vorticity and, as a consequence, the change in vorticity is larger than that indicated by the barotropic model.

Next, let us consider a thermal trough-ridge pattern which is out of phase by one quarter wavelength with the contour pattern. This is illustrated by figure 9. In figure 9 we may note that at the point of maximum cold advection (A'), the thermal vorticity (ζ_T) has a maximum. Similarly, B' represents a minimum for the thermal vorticity. At the centre of the trough (A),the term $V_T \cdot \nabla \zeta_T$ is negative because when we go along a segment (OO') of an isotherm, we go from high values of ζ_T to lower values. Hence,

$$\nabla \zeta_T \simeq \frac{\partial \zeta_T}{\partial s} \quad \text{is negative}$$

Moreover,

$$V_T > 0 \quad , \text{ so that}$$

$$V_T \cdot \nabla \zeta_T \simeq V_T \frac{\partial \zeta_T}{\partial s} < 0$$

The contribution of the thermal field to the development term

$\left(-\beta^2 V_T \cdot \nabla \zeta_T \right)$ is, therefore, positive.

By similar reasoning it can be shown that the contribution of the development term at B is negative. Hence, the thermal trough-ridge pattern, which lies upstream of the corresponding contour pattern, tends to increase cyclonic vorticity at A and decreases anticyclonic vorticity at B, that is, it tends to intensify the system. It can be similarly shown that when the thermal pattern lies downstream of the contour field, its effect is to weaken the system.

6.2.2 The prediction equations.

To derive a set of prediction equations we note that (6.2.1.5) gives us an expression for the change in vorticity at the mean level (m). A similar expression may be found for 1000mb. Lastly, from the first law of thermodynamics we can get an equation for the change in thickness between 1000 mb and the mean level (m). The point which has to be investigated is whether this set of three equations forms a closed set, i.e., whether the number of equations is sufficie to determine the total number of unknowns. The details are as follows.

On expanding the total time derivative of the potential temperature (θ), we get

$$\frac{1}{\theta}\frac{d\theta}{dt} = \frac{1}{\theta}\left(\frac{\partial\theta}{\partial t} + \mathbf{V}\cdot\nabla\theta\right) + \left(\frac{1}{\theta}\frac{\partial\theta}{\partial p}\right)\omega \qquad (6.2.2.1)$$

where ω is the vertical velocity in pressure co-ordinates. Making use of the equation for hydrostatic equilibrium (Haltiner and Martin, 1957), this may be expressed by

$$\frac{\partial}{\partial t}\left(\frac{\partial z}{\partial p}\right) = -\mathbf{V}\cdot\nabla\left(\frac{\partial z}{\partial p}\right) + \left(\frac{\alpha}{g\theta}\frac{\partial\theta}{\partial p}\right)\omega - \left(\frac{\alpha}{g\theta}\right)\frac{d\theta}{dt} \qquad (6.2.2.2)$$

Integration of the above between p_0 (1000 mb) and p_m yields

$$\frac{\partial h}{\partial t} = -\mathbf{V}_0\cdot\nabla h + \int_{p_0}^{p_m}\left(\frac{\alpha}{g\theta}\frac{\partial\theta}{\partial p}\right)\omega\, dp + Q \qquad (6.2.2.3)$$

where h is the thickness between p_m and p_0 and Q represents the change in thickness brought about by non-adiabatic heating or cooling. For simplicity, let us assume $Q = 0$, although the inclusion of Q is not difficult and can be carried out, if required. Let us also assume that $\left(\frac{\alpha}{g\theta}\frac{\partial\theta}{\partial p}\right)$ which is a measure of atmospheric stability, remains invariant with height. We may conveniently denote it by a stability parameter (σ).

In carrying out the integration of (6.2.2.2) it was tacitly assumed that (a) the contribution of V^{ir} is negligible and (b) $\mathbf{V}_T\cdot\nabla\left(\frac{\partial z}{\partial p}\right) = 0$. The second assumption is just another way of expressing the thermal wind equation. With these assumptions, we note that

$$\mathbb{V} \cdot \nabla \frac{\partial z}{\partial p} \simeq \mathbb{V}_m \cdot \nabla \left(\frac{\partial z}{\partial p} \right)$$

But,

$$\mathbb{V}_m = \mathbb{V}_o - \beta (o) \mathbb{V}_T \quad ,$$

So that,

$$\int_{p_o}^{p_m} \mathbb{V} \cdot \nabla \left(\frac{\partial z}{\partial p} \right) dp \simeq \mathbb{V}_o \cdot \nabla h$$

Incidentally, the above equation tells us that β (0), the value of β (p) at 1000 mb, is -1.

Having explained the principal assumptions in the model, we may express (6.2.1.5) and (6.2.2.3) by

$$\frac{\partial \zeta_m}{\partial t} = - \mathbb{V}_m \cdot \nabla (\zeta_m + f) - (\beta^2)_m \mathbb{V}_T \cdot \nabla \zeta_T \qquad (6.2.2.4)$$

$$\frac{\partial h}{\partial t} = - \mathbb{V}_o \cdot \nabla h - \sigma \omega \qquad (6.2.2.5)$$

To this we may also add the vorticity equation for 1000 mb

$$\frac{\partial \zeta_o}{\partial t} = - \mathbb{V}_o \cdot \nabla (\zeta_o + f) + f \left(\frac{\partial \omega}{\partial p} \right)_o \qquad (6.2.2.6)$$

The above represents a set of three equations for the four unknowns ζ_o, ζ_m, h and ω. We have, therefore, to reduce the number of unknowns by eliminating any one of the four. In most baroclinic models this is done by making an assumption, which fits in with reality, about the variation of ω with pressure. A convenient starting point is the equation of continuity. We have

$$\omega = - \int_{p_o}^{p} \nabla \cdot \mathbb{V} dp \qquad (6.2.2.7)$$

So far we have been only concerned with the non-divergent component of the wind, which makes no contribution to the divergence. The only contribution to the divergence comes from the irrotational component of the wind ($\mathbb{V}^{ir}$). We have so far assumed that the non-divergent part of the wind vector ($\mathbb{V}^{nd}$) could be expressed by

$$\mathbb{V}^{nd} = \mathbb{V}_m + \beta (p) \mathbb{V}_T$$

Is this assumption also valid for the irrotational part? Eliassen's model assumes that it is, so that the total divergence of $\mathbf{V}$ may be expressed by

$$\nabla \cdot \mathbf{V} = \nabla \cdot \mathbf{V}_m + \beta(p)\, \nabla \cdot \mathbf{V}_T \qquad (6.2.2.8)$$

If we make the further assumption that the wind vector at the mean level (m) is non-divergent, then

$$\nabla \cdot \mathbf{V} = \beta(p)\, \nabla \cdot \mathbf{V}_T \qquad (6.2.2.9)$$

Hence, on using (6.2.2.7) we have

$$\omega = -\int_{p_0}^{p} \beta(p)\, \nabla \cdot \mathbf{V}_T\, dp \simeq C(p)\, \nabla \cdot \mathbf{V}_T \qquad (6.2.2.10$$

where

$$C(p) = -\int_{p_0}^{p} \beta(p)\, dp \qquad (6.2.2.11$$

Substitution of the above result in (6.2.2.5) and (6.2.2.6) yields

$$\frac{\partial h}{\partial t} = -\mathbf{V}_0 \cdot \nabla h - \sigma C(p)\, \nabla \cdot \mathbf{V}_T \qquad (6.2.2.12$$

$$\frac{\partial}{\partial t}\left(\nabla^2 Z_0\right) = -\frac{f}{g}\mathbf{V}_0 \cdot \nabla\left(\frac{g}{f}\nabla^2 Z_0 + f\right) + \frac{f^2}{g}\nabla \cdot \mathbf{V}_T \qquad (6.2.2.13$$

where, in agreement with the geostrophic assumption, the surface vorticity is replaced by $\frac{g}{f}\nabla^2 Z_0$. We are now in a position to see the purpose behind the lengthy algebraic operations. Our primary objective was to remove one of the unknowns from the basic set of equations (6.2.2.4), (6.2.2.5) and (6.2.2.6). This is readily achieved if we eliminate thermal divergence $(\nabla \cdot \mathbf{V}_T)$ from (6.2.2.12) and (6.2.2.13). We have

$$\frac{\partial}{\partial t}\left[\nabla^2 Z_0 + \frac{f^2}{g\sigma C(p)}\, h\right] = -\frac{f}{g}\mathbf{V}_0 \cdot \nabla\left[\frac{g}{f}\nabla^2 Z_0 + f + \frac{f}{\sigma C(p)}\, h\right] \quad (6.2.$$

We may add to this (6.2.2.4),

$$\frac{\partial}{\partial t}\left(\nabla^2 Z_m\right) = -\frac{f}{g}\mathbf{V}_m \cdot \nabla\left[\frac{g}{f}\nabla^2 Z_m + f\right] - (\beta^2)_m\, \mathbf{V}_T \cdot \nabla\left(\nabla^2 h\right) \quad (6.2.$$

The above equations represent a closed set of two equations for the two unknowns Z(m) and Z(0). As these are the two basic parameters which we have to predict, this model is often called a two parameter model.

6.2.3 Graphical integration of the prediction equations.

The above prediction equations may be integrated graphically by Fjortoft's technique.

Thus, we may rewrite (6.2.2.14) as

$$\frac{\partial}{\partial t}\left(\bar{Z}_o - Z_o + \phi h + G\right) = -\mathbf{V}_o \cdot \nabla\left(\bar{Z}_o - Z_o + \phi h + G\right) \qquad (6.2.3.1)$$

Where

$$G = \left(\frac{H}{m}\right)^2 \frac{f^2}{g}$$

$$\phi = \frac{f^2}{g\sigma C}\left(\frac{H}{m}\right)^2$$

H = the distance between two modal points of the unit grid and

$$\bar{Z}_o = \frac{1}{4}\left[\sum_1^4 Z_o\right]$$

The advecting velocity $\mathbf{V}_o$ is too unsteady for practical use. In agreement with Fjortoft's technique we could replace it by a steadier velocity $\overline{\mathbf{V}_o}$, where $\overline{\mathbf{V}}_o = \mathbf{k} \times \nabla \bar{Z}_o$ But, the process of integration would still be tedious. We can, however, shorten the work by a useful short-cut proposed by Sanders (1959).

The right hand side of (6.2.3.1) contains the terms

$$-\mathbf{V}_o \cdot \nabla \bar{Z}_o \;;$$

$$+\mathbf{V}_o \cdot \nabla Z_o \;;$$

$$-\phi\, \mathbf{V}_o \cdot \nabla h \quad \text{and}$$

$$-\mathbf{V}_o \cdot \nabla G$$

The second term presents no problems because it is identically zero. An appeal to orders of magnitude reveals that the contribution of $\phi\, \mathbf{V}_o \cdot \nabla h$ is the largest; the others are generally small by comparison. Secondly, we may note that:

$$\mathbf{V}_o \cdot \nabla Z_m = (\mathbf{V}_m - \mathbf{V}_T) \cdot \nabla (z_o + h)$$

or

$$\mathbf{V}_o \cdot \nabla Z_m = \mathbf{V}_m \cdot \nabla Z_o - \mathbf{V}_T \cdot \nabla Z_o + \mathbf{V}_m \cdot \nabla h$$

$$= -\mathbf{V}_m \cdot \nabla Z_o$$

because $\mathbb{V}_m \cdot \nabla Z_m = \mathbb{V}_o \cdot \nabla Z_o = 0$. On using the above identity and only retaining the term $\phi \mathbb{V}_o \cdot \nabla h$ on the right hand side of (6.2.3.1) we get

$$\frac{\partial}{\partial t}\left[\bar{Z}_o - (1+\phi) Z_o\right] = \phi \mathbb{V}_m \cdot \nabla Z_o - \phi \frac{\partial Z_m}{\partial t} \qquad (6.2.3.2)$$

The value of ϕ depends on the length of the unit grid (H), but if this is chosen suitably such that $\phi < 1$, then, as a first approximation, we may replace the left hand side of (6.2.3.2) by $-\frac{\partial Z_o}{\partial t}$. Equation (6.2.3.2) thus gives us a convenient expression for the tendency at 1000 mb, if we can find a suitable value for ϕ. Now,

$$\phi = \frac{f^2}{g\sigma C}\left(\frac{H}{m}\right)^2$$

using representative values for the atmosphere, the factor

$$\frac{f^2}{g\sigma C} \simeq 10^{-15}\ \text{cm}^{-2}$$

This factor remains invariant, so that the only parameter which determines ϕ is the choice of the unit grid interval (H). A suitable value would be to set

$$\frac{H}{m} \simeq 250\ \text{km},$$

so that

$$\phi \simeq 0.5$$

This would reduce (6.2.3.2) to

$$-\frac{\partial Z_o}{\partial t} = \frac{1}{2}\mathbb{V}_m \cdot \nabla Z_o - \frac{1}{2}\frac{\partial Z_m}{\partial t} \qquad (6.2.3.3)$$

Equation (6.2.3.3) gives us a fairly simple and convenient method for computing $\frac{\partial Z_o}{\partial t}$. We have to only advect the field of Z_o by half the 500 mb wind vector and substract half the tendency at 500 mb to get the tendency at 1000 mb. It is important to note that this will work best only for disturbances of one particular wave length, determined by our choice of H, and consequently, of ϕ This wave length is of the order of 2000 km.

We have been so far concerned with the prediction of the 1000 mb contours. We shall next consider prediction of the intensification or weakening of pressur

systems. It will be noted that (6.2.1.5) is identical with the barotropic vorticity equation, but for the last term which indicates the weakening or intensification of the system under consideration. For practical purposes it is convenient to evaluate this term only at points where the advection of absolute vorticity is zero, i.e., at the inflexion points of troughs, ridges, highs and lows of the contour pattern.

At such points

$$\frac{\partial z_m}{\partial t} = -(\beta^2)_m \mathbf{V}_T \cdot \nabla(\nabla^2 h) \qquad (6.2.3.4)$$

Let us now define a new field $\bar{h}$, in the same way as we defined $\bar{Z}$, and let

$$\overline{\mathbf{V}}_T = \mathbf{k} \times \nabla \bar{h}$$

Then,

$$\mathbf{V}_T \cdot \nabla(\nabla^2 h) = (\mathbf{V}_T + \overline{\mathbf{V}}_T) \cdot \nabla(h - \bar{h}) = \overline{\mathbf{V}}_T \cdot \nabla h ,$$

whence

$$\frac{\partial z_m}{\partial t} = -(\beta^2)_m \overline{\mathbf{V}}_T \cdot \nabla h \qquad (6.2.3.5)$$

For operational purposes, the correction term can be readily evaluated by choosing a suitable value for $(\beta^2)_m$ and by drawing the isopleths of h. From these isopleths, $\bar{h}$, $\overline{\mathbf{V}}_T$ may be constructed in the same way as in Fjortoft's technique.

6.2.4 Practical steps for using the prediction equations.

The mean level of the atmosphere is usually indentified with 500 mb, but in actual practice it is nearer to 600 mb. Thus, the development term is strictly valid at 600 mb, while we have to work in practice with 500 mb. The difficulty is partially removed if we note that

$$\mathbf{V}_5 = \mathbf{V}_6 + \beta(5)\mathbf{V}_T^6$$

$$\mathbf{V}_0 = \mathbf{V}_6 + \beta(0)\mathbf{V}_T^6 = \mathbf{V}_6 - \mathbf{V}_T^6$$

Hence,

$$\mathbf{V}_5 - \mathbf{V}_0 = \mathbf{V}_T^5 = [\beta(5) + 1]\mathbf{V}_T^6 .$$

$$\zeta_T^5 = [\beta(5) + 1]\,\zeta_T^6$$

Consequently,

$$V_T^6 \cdot \nabla \zeta_T^6 = \frac{1}{[\beta(5)+1]^2}\, V_T^5 \cdot \nabla \zeta_T^5$$

Substitution in (6.2.3.4) gives us

$$\frac{\partial Z_5}{\partial t} = - \frac{(\beta^2)_m}{[\beta(5)+1]^2}\, V_T^5 \cdot \nabla\, \zeta_T^5 \qquad (6.2.4.1)$$

The normal upper winds of the world have been tabulated by Buch. From Buch's normal data we find that

$$\frac{(\beta^2)_m}{[\beta(5)+1]^2} \simeq 0.34 \qquad (6.2.4.2)$$

Hence,

$$\frac{\partial Z_5}{\partial t} = - 0.34\, \overline{V}_T^5 \cdot \nabla h \qquad (6.2.4.3)$$

The integration of the above equation is now straightforward. Suppose we wish to integrate it over a time interval of $2\Delta t$. We have

$$(Z_5)_{t+2\Delta t} - (Z_5)_t = (-0.34\, \overline{V}_T^5 \cdot \nabla h) \times 2\Delta t \qquad (6.2.4.4)$$

For a 24 hour forecast, Δt = 12 hours. Consequently, we displace the contours of h by the wind and find out the distance traversed in

$$0.34 \times 2 \times 12 \simeq 8 \text{ hours}$$

This will give us the correction to be applied to the barotropic forecast.

Sanders (1959) has indicated a slightly different procedure, but the difference is very small. If we make the assumption that

$$\frac{\partial h}{\partial t} = - 0.34\, \overline{V}_T^5 \cdot \nabla h \,,$$

then it follows that

$$h_{t+\Delta t} - h_{t-\Delta t} = (-0.34\, \overline{V}_T^5 \cdot \nabla h) \times 2\Delta t$$

Now, $h_{t+\Delta t}$ is obtained by displacing the isopleths of h a distance downstream corresponding to $0.34 \times \Delta t$ i.e., 4 hours for a 24 hour forecast.

Similarly, $h_{t-\Delta t}$ is obtained by displacing the contours of h a corresponding distance upstream. The difference gives us the required correction term.

To sum up, the different steps may be summarized as follows.

a) Prepare a 500 mb forecast by Fjortoft's technique, or any other suitable method.

b) On a separate chart draw isopleths of the thickness between 1000–500 mb.

c) From isopleths of h, prepare the field of h by the technique given in the discussion of Fjortoft's method.

d) At all points of interest, evaluate $\overline{|V_T|}^5$ from the $\bar{h}$ chart. Displace contours of h by $\overline{V_T}^5$ and find the distance traversed in 8 hours. The negative of this quantity is to be added to the Z field to get new contours of the 500 mb surface.

e) Sander's alternative procedure would be to first displace the contours of h downstream by $\overline{V_T}^5$ corresponding to a time interval of 4 hours. Next, the contours may be displaced upstream by the same amount. The difference gives the correction for development.

6.2.5 Comparison of Eliassen's model with other baroclinic models.

It may be of interest to indicate a few comparative notes between Eliassen's model, which we have described, with a few other baroclinic models. As mentioned earlier, the difference between different baroclinic models is small; it mainly lies in the manner in which we assume the vertical velocity to vary with pressure.

Eliassen's model assumes that

$$\nabla \cdot V = \beta(5)\, \nabla \cdot V_T \quad , \qquad (6.2.5.1)$$

whence

$$\left(\frac{\partial \omega}{\partial p}\right)_0 = -\beta(0)\, \nabla \cdot V_T = \nabla \cdot V_T \qquad (6.2.5.2)$$

The variation of $\beta(p)$ with pressure can be determined from Buch's values of the mean wind over different parts of the globe. Most baroclinic models

assume that ω varies parabolically with pressure. Thus Estoque (1955) assumes

$$\omega = \sqrt{2}\ \omega_m\ \mathrm{Sin}\ \frac{\pi}{2}\ \frac{p_o - p}{p_o - p_m}\ , \qquad (6.2.5.3)$$

whence

$$\left(\frac{\partial \omega}{\partial p}\right)_{p=p_o} = -\frac{\pi}{\sqrt{2}}\ \frac{\omega_m}{p_o - p_m} \qquad (6.2.5.4)$$

Comparing (6.2.5.4) with (6.2.5.2) we see that

$$\nabla \cdot \mathbf{V}_T = -\frac{\pi}{\sqrt{2}}\ \frac{\omega_m}{p_o - p_m}$$

But,

$$\omega = -\int_{p_o}^{p} \beta(p)\, \nabla \cdot \mathbf{V}_T\, dp\ ,$$

$$= \frac{\pi}{\sqrt{2}}\ \frac{\omega_m}{p_o - p_m} \int_{p_o}^{p} \beta(p)\, dp \qquad (6.2.5.5)$$

Equating (6.2.5.5) with (6.2.5.3) we get

$$\int_o^p \beta(p)\, dp = \frac{2}{\pi}(p_o - p_m)\ \mathrm{Sin}\ \frac{\pi}{2}\ \frac{p_o - p}{p_o - p_m}$$

On carrying out the integration, we have

$$\beta(p) = -\mathrm{Cos}\ \frac{\pi}{2}\ \frac{p_o - p}{p_o - p_m} \qquad (6.2.5.6)$$

In Sawyer and Bushby's model (1953), the vertical velocity profile is

$$\omega = \omega_m (1 - \alpha^2) \qquad (6.2.5.7)$$

where

$$\alpha = \frac{p_m - p}{p_o - p_m}$$

It is clear that their α is identical with $\beta(p)$ of Eliassen's model. Let us, therefore, compute using equations (6.2.5.6) and (6.2.5.7) and see how they compare with Buch's values for different pressures. The comparison is shown in Table IV.

TABLE - IV

Values of β (P) for different models

Pressure (mb)	Value of $\beta(P)$		
	Buch	Estoque	Sawyer and Bushby
1000	-1.00	-1.00	-1.00
900	- .79	- .92	- .75
800	- .52	- .71	- .50
700	- .29	- .38	- .25
600	- .02	- .00	- .00
500	+ .24	+ .38	+ .25
400	+ .47	+ .72	+ .50
300	+ .68	+ .92	+ .75
200	+ .80	+1.00	+1.20
100	+ .44	+ .38	+1.25
0	-1.08	+ .71	+1.50

The table shows that both the models of Estoque and Sawyer and Bushby fit the observed values of Buch fairly well, except at levels higher than 200 mb. All the profiles change sign, as expected, at the level of the mean wind (600 mb).

6.3 The anomaly technique

6.3.1 Introduction.

Recent studies in the tropics have shown that the lower tropospheric circulations and their development are substantially controlled by the divergence and convergence associated with upper tropospheric waves, (1968). Dines' thesis that the sign of divergence usually changes once in the vertical (1919) has received considerable support in recent years from numerous investigations. There is increasing evidence of the existence of a level of minimum divergence

in the tropical troposphere in the vicinity of 500 mb. Theoretical models of the troposphere formulated purely on the basis of geostrophic approximations at the level of non-divergence do not include orographical,geographical and seasonal variations, as their incorporation into prediction equations would render them unwieldy. Climatological models would, however, accommodate all parameters, which have a modifying influence on meteorological situations. A climatological normal of a parameter at a point represents the statistical time-mean of all the elements at that point. The departure at a given time at that point from its normal value is its "anomaly". Synoptic charts displaying the fields of departure from normal over a given area would, therefore, portray meteorological patterns, from which all local and seasonal effects are excluded. Experience in the tropics shows that the departures from normal even of sea-level pressure constitutes a powerful diagnostic tool in the hands of the tropical meteorologist.

The patterns of pressure anomaly at 500 mb, where conditions may be assumed for operational simplicity to be barotropic, will closely correspond to the vorticity patterns. Anomaly patterns can therefore be advected in the time-mean contour field in the same manner as vorticity patterns in the space-mean contour field over relatively short periods of prognosis such as of 12 to 24 hours. A simple and objective prognostic technique for construction of barotropic prognostic charts based on contour height anomalies at the 500 mb. level is described here.

6.3.2 The prediction equation

The pressure tendency $\frac{dp_o}{dt}$ at any point on an isobaric surface may be identified,on considerations of continuity, with the vertical velocity of a moving particle relative to the isobaric surface. If there is isobaric convergence between a level designated as P_o and a higher level say P_1 then

$$\frac{dp_o}{dt} = -\int_{p_1}^{p_o} \nabla p \cdot W \, \partial p$$

where $\mathbb{V}$ the wind vector.

If the upper level is the top of the atmosphere such that $p_1 = 0$, then we may write

$$\frac{dp_o}{dt} = -\int_o^{p_o} \nabla_p \cdot \mathbb{V} p \qquad (6.3.1.1)$$

Expanding $\frac{dp_o}{dt}$ and dropping the subscript o

$$\frac{\partial p}{\partial t} + \mathbb{V} \cdot \nabla_H p + \omega \frac{\partial p}{\partial z} = -\int_o^p \nabla_p \cdot \mathbb{V} \, \partial p \qquad (6.3.1.2)$$

where ω is the vertical velocity at the pressure level p.

Substituting for p in terms of Z to convert pressure tendencies into height tendencies at a constant level to facilitate contour analysis, we get, using conventional symbols,

$$\frac{\partial z}{\partial t} = \frac{1}{g\rho} \int_o^p \nabla_p \cdot \mathbb{V} \, \delta p - \mathbb{V} \cdot \nabla_p \, z - \omega \qquad (6.3.1.3)$$

The first term on the right represents isobaric divergence, the second advection of the height field and the last vertical velocity through the isobaric surface. Let us now make the following assumptions:

1. The conditions at the 500 mb level are quasi-barotropic, so that the geostrophic vorticity and height changes at this level are conserved. The first term on the right of equation (6.3.1.3) may, therefore, be dropped.
2. The vertical velocity through the isobaric surface is smaller by at least one order of magnitude than the geostrophic wind at the 500 mb level, so that this can be ignored by comparison with the advection term.

We may, therefore, recast equation (6.3.1.3) as

$$\frac{\partial z}{\partial t} = -\mathbb{V} \cdot \nabla_{500} z \quad \text{or simply} \quad -\mathbb{V} \cdot \nabla \, z \qquad (6.3.1.4)$$

To get contour height tendencies in terms of contour height anomalies, let us put

$$\alpha = z - N \qquad (6.3.1.5)$$

where N and a respectively represent the normal height of this isobaric

surface and anomaly of the normal height of the surface.

From (6.3.1.5) we may write

$$\frac{\partial a}{\partial t} = \frac{\partial z}{\partial t} - \frac{\partial N}{\partial t}\ ,\ \frac{\partial a}{\partial x} = \frac{\partial z}{\partial x} - \frac{\partial N}{\partial x} \quad \text{and} \quad \frac{\partial a}{\partial y} = \frac{\partial z}{\partial y} - \frac{\partial N}{\partial y}$$

As the normal height value is invariant with time,

$$\frac{\partial N}{\partial t} = 0 \quad \text{and} \quad \frac{\partial a}{\partial t} = \frac{\partial z}{\partial t}$$

so that

$$\frac{\partial a}{\partial t} = -\left[u\left(\frac{\partial a}{\partial x} + \frac{\partial N}{\partial x}\right) + v\left(\frac{\partial a}{\partial y} + \frac{\partial N}{\partial y}\right)\right]$$

$$= -\frac{g}{f}\left[\left(-\frac{\partial z}{\partial y}\frac{\partial a}{\partial x} + \frac{\partial z}{\partial x}\frac{\partial a}{\partial y}\right)\right] - \left(u\frac{\partial N}{\partial x} + v\frac{\partial N}{\partial y}\right)$$

$$= -\frac{g}{f} J(z, a) - \left(u\frac{\partial N}{\partial x} + v\frac{\partial N}{\partial y}\right) \qquad (6.3.1.6)$$

In the last term on the right, u and v are the zonal and meridional components of the horizontal wind vector. As the normal contours run almost parallel to the latitude circles $\frac{\partial N}{\partial x}$ is negligible in magnitude and may be ignored. The value of $v\frac{\partial N}{\partial y}$ may be of either sign along a trajectory and its integrated effect over a long interval of time such as 12 or 24 hours is likely to become negligible. In an extreme instance of the passage of a well-marked trough or ridge-line across a point symmetrically in space and time, the meridional component may be reversed so as to reduce this term to zero. The term $v\frac{\partial N}{\partial y}$ may, therefore, be neglected, especially relative to the Jacobian.

We may, therefore, rewrite 6.3.1.6 as

$$\frac{\partial a}{\partial t} = -\frac{g}{f} J(z, a) = -\frac{g}{f} J(z, z-N)$$

$$= -\frac{g}{f} J\left[z - (z-N), (z-N)\right]$$

$$= -\frac{g}{f} J(N, z-N) \qquad (6.3.1.7)$$

where $z - N = a$ is the advected quantity and N is the advecting field. The

map scale factor arising as a result of transition from the sphere to the actual map would affect both sides of the above equality in the same ratio and does not, therefore, enter the equation.

The prognostic anomaly field 'a' at the end of a prognostic period 't' would, on graphical subtraction from the initial anomaly field 'a_o' represent the change in the anomaly pattern over the period 't'. The difference between the two fields, that is $(a_t - a_o)$, would yield the Z_t chart representing the contours at the end of the period 't' on graphical addition to Z_o field. Experience, however, shows that the results obtained by direct graphical addition of the prognostic anomaly field 'a_t' to the normal field N in one single step are substantially identical with those achieved in the above three steps.

6.3.3 Operational procedure

Preparation of the prognostic 500 mb chart by the contour anomaly technique is accomplished by advecting the anomaly field for the 12 or 24 hour prognostic period with the mean normal geostrophic wind corresponding to the N field and adding the advected anomaly field to the N field. Given a short-period, preferably 5 day or 10 day normal contour field, time-centred on the analytical chart used, the prognostic chart can be constructed in three simple steps as follows:

Step 1 : Subtract graphically the 'N' field from the 'Z' field to get the 'a' field.

Step 2 : Advect the 'a' field over the prognostic period 't' in the 'N' field to get the 'a_t' field.

Step 3 : On a blank map, add graphically the advected ('a_t') field to the 'N' field to obtain the prognostic 500 mb chart.

As an album of short-period normal charts can be kept permanently ready for use, the time involved in preparing the prognostic 500 mb chart is merely that required for the graphical subtraction, construction of the advected field and graphical addition of the latter to the normal. Further economy in time can be

secured in Step 2 by plotting on the normal charts numbers showing the displacement in degrees latitude corresponding to the normal contour field for a 24-hour prognostic period as spot-values at each 10° intersection of latitude and longitude. With the help of such a spot-value normal contour chart for a short 5 or 10 day period, the contour anomaly technique can be used to prepare objective numerical prognostic charts for the 500 mb level in less than half-an-hour from the time the analysed 500 mb chart is available.

6.3.4 The anomaly technique has yielded equally striking results in all the seasons of the year. As the normals are for a long period of one month at a stretch, the 500 mb normal charts have been treated as time-centred on the 15th of the month to which they pertain. Prognostic charts prepared by the anomaly technique on the middle dates of the months of January, March, July and October compared quite favourably with those prepared by the Fjortoft technique. The results could doubtless have been better if normal charts for shorter periods wer employed.

6.3.5 Limitations of the technique

The technique developed here is based primarily upon the assumption that the current 500 mb contours may be visualised as being composed of certain migratory synoptic-scale disturbances superimposed upon a normal contour configuration. It is, therefore, liable to failure to the extent to which this assumption fails to hold.

Let us consider critically the relationship that anomaly patterns bear to vorticity patterns. As $a = Z - N$, we may write

$$a + \bar{Z} = Z + \bar{Z} - N \qquad (6.3.1.8)$$

where $\bar{Z}$ is the space-mean of the 500 mb contour heights used in the Fjortoft technique.

We may re-write (6.3.1.8) as

$$a = (Z - \bar{Z}) + (\bar{Z} - N)$$

which show that the anomaly is made up of (1) the relative vorticity or $(Z - \bar{Z})$ with sign reversed, representing the synoptic scale disturbances and (2) the anomaly of the space-mean contours. The anomaly would truly represent the relative vorticity field or $a = -(Z - \bar{Z})$ only when $(\bar{Z} - N) = 0$, or the space-mean chart is devoid of space-mean troughs and ridges. If, however, the space-mean contour field is anomalous or displays troughs and ridges, the vorticity patterns tend to appear more accentuated than the contour anomaly patterns. In other words, the contour-anomaly technique would yield prognostic charts with weaker gradients than those displayed in the Fjortoft prognostic charts in regions where there are long wave troughs and ridges.

6.3.6 Advantages of the anomaly technique.

The anomaly patterns obtained by subtracting out the normal contours, which constitute a major part of the isobaric chart, portray the short-wave disturbances as closed centres of negative and positive anomalies more conspicuously than the vorticity patterns obtained by subtracting out the space-mean contours. Secondly, the anomaly patterns reveal ridges in areas where quasi-stationary space-mean and normal contour troughs occur as positive anomaly centres, while vorticity charts may not locate and portray such features. An instance in point is the persistent trough, which occurs off the Asian coast in winter where vorticity ridges tend to lose their identity on arrival. Thirdly, the anomaly patterns are relatively more useful than vorticity patterns for preparing graphical prognostic charts in regions where latitudinally-oriented large-scale elliptical patterns, which cannot be classed as troughs or ridges, occur in contour maps. Finally, the marginal errors, which arise in preparing charts by the Fjortoft technique on account of displacements of charts along both the horizontal axes for preparing the space-mean charts, would not appear in the charts prepared by the anomaly technique, as this does not involve such displacements.

6.3.7 Subjective adjustments.

The anomaly technique yields successful results in the areas of the chart north of 30°N where the geostrophic approximations and assumptions of advection involved in the prognostic equation are largely justified. During the winter period when the atmospheric processes are mainly advective and the prediction equation based on the assumption of quasi-horizontal displacement of pressure patterns holds even upto latitude 15°N, satisfactory prognostic charts can be constructed upto very low latitudes. In areas further to the south, the prognostic contours could be delineated by extrapolation from the objective prognostic contours at the higher latitudes. The final charts would, in any case, have to be refined subjectively keeping the principles of continuity in time, consistency in the vertical and coherence with the developments during the prognostic period, deducible from other considerations, in view.

6.4 Discussion of methods suitable for low latitudes.

We have been hitherto concerned with methods of prognosis which were largely developed for extra-tropical latitudes. It has to be admitted at the outset that research on similar prognostic techniques for low latitudes is still in an experimental stage.

The main difficulty in low latitudes is the lack of geostrophic balance and, as a consequence, the absence of a reliable relation between the wind and pressure. An additional difficulty is the absence of an adequate coverage of aerological data. This makes it difficult for an analyst to draw any kind of isopleth with confidence. Notwithstanding these limitations, a considerable amount of experimental work is in progress to apply our theoretical knowledge to the special problems of tropical meteorology. The purpose of the present section is to review a few methods and techniques, which appear to show some promise towards the ultimate development of an operationally feasible technique.

6.4.1 Grimes' method of dynamic pressure.

Grimes (1951) introduced the dynamic pressure in an attempt to derive a

wind-pressure relationship suitable for the tropics. The dynamic pressure (P) is defined by

$$P = p + \tfrac{1}{2} v^2 \qquad (6.4.1.1)$$

where p is the pressure, $v^2 = u^2 + v^2$ and u,v are the zonal and meridional components of wind.

With the above definition of P, the equations of motion may be expressed by,

$$\frac{\partial u}{\partial t} - Kv = -\frac{1}{\rho}\frac{\partial P}{\partial x}, \qquad (6.4.1.2)$$

$$\frac{\partial v}{\partial t} + Ku = -\frac{1}{\rho}\frac{\partial P}{\partial y}, \qquad (6.4.1.3)$$

where

$$K = \zeta + f$$

ζ is the vertical component of vorticity and

f is the Coriolis parameter

Equation (6.4.1.2) and (6.4.1.3) do not involve any assumptions, except for the neglect of friction. It follows from the above equations that for steady, unaccelerated motion, we have

$$u = -\frac{1}{\rho K}\frac{\partial P}{\partial y} \qquad (6.4.1.4)$$

$$v = \frac{1}{\rho K}\frac{\partial P}{\partial x} \qquad (6.4.1.5)$$

The above equations represent a modified form of the geostrophic relationship between isopleths of P and components of the wind (u,v). This also has an interesting interpretation to which Kruger (1960) has recently drawn attention.

We can see from (6.4.1.4) and (6.4.1.5) that the direction of the wind will be directly opposed to P, if K becomes negative. This will happen when

$$-\zeta > f,$$

or the anticyclonic vorticity exceeds the coriolis parameter. This type of flow is often called an "antiflow", and Kruger (Loc. cit) has furnished examples from the equatorial regions of Africa.

For non-divergent motion, we can make use of the familiar vorticity equation in the form

$$\frac{dK}{dt} = 0 \qquad (6.4.1.6)$$

from which it follows that K is constant along a trajectory. If we can draw the isopleths of P with reasonable accuracy, then the constant K can be fixed by the use of a geostrophic wind scale. Let

$$K = 2\Omega \sin\phi + \zeta = 2\Omega \sin\phi' \quad \text{(say)} \qquad (6.4.1.7)$$

then the appropriate value of ϕ' may be obtained from the geostrophic wind scale. Hence,

$$\zeta = 2\Omega (\sin\phi' - \sin\phi) \qquad (6.4.1.8)$$

This gives us a quick and easy method of determining the regions of cyclonic and anticyclonic vorticity.

In actual practice it was found that the main difficulty of this method lay in drawing reliable isopleths of P, particularly over southeast Asia. With improvement in telecommunications and availability of upper air data, it is not unlikely, however, that this mode of approach will be developed further.

6.4.2 Methods of prognosis based on the wind field.

Generally a vector, such as the wind, can be resolved into two components, namely, (a) a part which is non-divergent and (b) a component which has divergen but no rotation (vorticity). The wind vector may then be formally expressed by

$$V = \mathbf{k} \times \nabla\psi + \nabla\phi \quad , \qquad (6.4.2.1)$$

where $\mathbf{k}$ is the unit vector along the vertical, ψ is a stream function and ϕ is a velocity potential. Experience suggests that the irrotational component is usually small compared to the non-divergent part, so that for practical purposes we can represent the wind components by the gradient of a stream function.

We have

$$u = -\frac{\partial\psi}{\partial y} \qquad (6.4.2.2)$$

$$v = \frac{\partial\psi}{\partial x} \qquad (6.4.2.3)$$

whence

$$\zeta = \frac{\partial v}{\partial x} - \frac{\partial u}{\partial y} = \nabla^2 \psi$$

and $$\nabla^2 = \frac{\partial^2}{\partial x^2} + \frac{\partial^2}{\partial y^2} \qquad (6.4.2.4)$$

If we resolve the available wind data into u and v components, and evaluate ζ as a function of the x and y coordinates, say F(x,y), then the stream function may be obtained by solving the Poisson's equation,

$$\nabla^2 \psi = F(x, Y) \qquad (6.4.2.5)$$

The solution of Poisson's equation can be obtained by relaxation or by analytical methods, but we will need a suitable boundary condition. For convenience, we may assume

$$\psi = o$$

or $$\frac{\partial \psi}{\partial s} = V_n$$

along the boundary. The subscript n denotes the component normal to the boundary, and δs represents a segment of the boundary.

The above outline of a possible technique for the tropics is indicated here, because it is possible to express the vorticity equation in terms of ψ and to integrate it by graphical methods.

It is, of course, possible to represent the wind field by more sophisticated methods, but the resulting equations become more complicated. Briefly the technique is to take the divergence of the equation of motion. This gives us the divergence equation, which contains both the divergence, and the vorticity, and also the time derivative of the divergence.

The full equation is

$$\frac{dD}{dt} + D^2 + \left(\frac{\partial \omega}{\partial x}\frac{\partial u}{\partial p} + \frac{\partial \omega}{\partial y}\frac{\partial v}{\partial p}\right) = -g\nabla^2 Z + f\zeta - \beta v + Z\left(\frac{\partial u}{\partial x}\frac{\partial v}{\partial y} - \frac{\partial u}{\partial y}\frac{\partial v}{\partial x}\right), \qquad (6.4.2.6)$$

where

$$D = \nabla \cdot V$$

By considering orders of magnitude it can be shown that all the terms on the left hand side of (6.4.2.6) are at least one order of magnitude smaller than those on the right hand side. Consequently, if they are neglected, we are left with

$$\zeta + \frac{z}{f}\left(\frac{\partial u}{\partial x}\frac{\partial v}{\partial y} - \frac{\partial u}{\partial y}\frac{\partial v}{\partial x}\right) + \frac{\beta\omega}{f} = \frac{g}{f}\nabla^2 z$$

In terms of streamfunction (Ψ) this reduces to

$$\nabla^2\psi + \frac{z}{f}\left[\frac{\partial^2\psi}{\partial x^2}\frac{\partial^2\psi}{\partial y^2} - \left(\frac{\partial^2\psi}{\partial x\,\partial y}\right)^2\right] + \beta\frac{\partial\psi}{\partial x} = \frac{g}{f}\nabla^2 z \qquad (6.4.2.7)$$

If we are given the field of Z, then theoretically we should be able to obtain Ψ. But, there is no easy analytical solution on account of the mixed derivatives on the lefthand side.

6.4.3 Synoptic examples of low pressure systems in low latitudes.

A systematic synoptic study of low pressure systems, which move westwards from the south China sea to the Arabian Sea across the southern half of the Indian Peninsula, has recently become possible with improved telecommunication facilities Although the number of cases studied has been rather limited so far, a few tentative results are presented below in view of their importance for flights south of 30°N.

The main characteristics of these low pressure systems may be summarised as follows:-

i) The flow pattern at 300 mb appears to follow a sinusoidal pattern in the monsoon months. The troughs and ridges appear to form closed vortices, in the form of lows and highs, at lower levels. During the monsoon months these vortices are often masked by the main monsoon current, but in winter and the post-monsoon period they can be fairly readily discerned.

ii) The lateral spacing between successive troughs is of the order of 15-20 degrees longitude. The spacing appears to remain fairly constant for a number of days before exhibiting a sudden breakdown, or movement westwards.

iii) Prior to a breakdown or rapid westward movement, the zonal wind, which is easterly and generally weak, strengthens to above 20 knots.

iv) The normal movement westwards appears to be of the order of 2 to 4 degrees longitude per day. In view of the weak zonal current and the small wave length, the application of Rossby's formula does not appear to indicate encouraging results.

v) The thermal field associated with these migratory systems is usually weak.

We have in the foregoing indicated a few practical suggestions for low latitudes. As stated earlier, these methods are in an experimental stage. With improved coverage of data it should be possible, in the next few years, to try out such methods more extensively. It is then that we hope an operationally feasible method of prognosis, which is not entirely subjective, will emerge.

REFERENCES

1. Charney, J.G. and Phillips, N.A. 1953: Jour. Met., Washington, 10,2,191

2. Eady E.T. 1952: Tellus, 4, 157.

3. Eliassen, A. 1956: Univ. California, Dept. Met., Sci. Rept. No.4.

4. Estoque, M.A. 1955: Univ. Chicago, Dept. Met., Tech. Rept. No.5.

5. Grimes, A. 1951: Compendium of Meteorology, Amer. Met. Soc., Washington, 881.

6. Kruger, E. 1959: Generalized gradient wind equations and contour analysis in the tropics. / Tropical Met. in Africa, Proc. [illegible] Foundation Symposium, 168-177 176. / Symposium on

7. Sawyer, J.S. and Bushby, F.H. 1953: Jour. Met., Washington, 10,54.

8. Sanders, F. 1959: Lecture Notes, Dept. Met., Mass. Inst. Techy., Cambridge, Mass., USA.

Chapter 7

Objective assessment of the accuracy of forecasts

Many attempts have been made in recent years to find an objective system of verifying the correctness of predicted height (or pressure) changes. This problem, which at first sight seems straightforward, is extremely complicated because there is no accepted criterion of what constitutes an objective assessment. In this review, therefore, we shall describe the different tests which have been generally employed. A preliminary report on the application of some of these tests on the prognostic charts prepared at Northern Hemispheric Analysis Centre, New Delhi, will be provided at the end.

7.1 Correlation Coefficients.

In most statistical work, the correlation co-efficient is widely used to measure the association between computed and predicted height changes. However, the correlation co-efficient by itself does not correctly represent the efficiency (or skill) of the forecasting technique, because different factors, such as, persistence or the speed with which a system moves, give an undue bias to the correlation coefficient.

A system which moves slowly would yield a higher correlation between predicted and observed height changes than a fast moving system. Thus, a certain amount of undue credit would be given to poor forecasts for slow moving systems, and a good forecast would be discredited if the system was a fast moving one. Petterssen (1957) illustrated this by considering a sinusoidal pressure wave travelling along the x-axis. The wave profile at any instant may be represented by

$$Y_o = A \sin \frac{2\pi}{L} (x - ct) + No \qquad (7.1.1)$$

Where L is the wave length, c the phase velocity and A is the amplitude of the wave. By 'No' we represent a field of error or 'noise', caused by limitations of our observational technique. This is taken to be superimposed

on the fundamental wave. Suppose we make two observations of the wave profile at times t_o and $t_{o+\Delta t}$, then it can be readily shown that (ΔY_o) takes on different values depending on the magnitude of $c\Delta t$. If we consider the case of (a) $c\Delta t = \frac{L}{2}$ and (b) $c\Delta t = L$, then

(a) gives as

$$(Y_o)_1 = A \sin \frac{2\pi x}{L} + (No)_1$$

$$(Y_o)_2 = -A \sin \frac{2\pi x}{L} + (No)_2$$

or $$\Delta Y = -2A \sin \frac{2\pi x}{L} + \Delta No \qquad (7.1.2)$$

Similarly, for (b) we have

$$(Y_o)_1 = A \sin \frac{2\pi x}{L} + (No)_1$$

$$(Y_o)_2 = A \sin \frac{2\pi x}{L} + (No)_2$$

or $$\Delta Y_o = \Delta No \qquad (7.1.3)$$

We can make the reasonable assumption that the amplitude of the wave pattern(A) is considerably greater than the noise (No.). From equations(7.1.2) and (7.1.3) we can see that we shall get a high or low correlation (between predicted and observed height changes) depending on whether the forecast interval is $\frac{L}{2}$ or L. When the interval is less than L (7.1.2), a higher correlation would be expected because the wave amplitude is greater than No. But when the interval is L (7.1.3), the height change is entirely determined by the noise (No), and a low correlation would be the result.

7.2 Skill Scores.

Because the correlation coefficient is biased by persistence and the speed of the system, a number of skill scores have been designed to supplement the correlation coefficient. One such skill score, defined by Petterssen(1957) tries to eliminate the effect of persistence by using the initial chart as the prognostic chart. The underlying idea is to see what correlation is obtained, if we had made no attempt at prediction, but simply used the initial chart as the prognosticated one. The skill score is then defined as

$$S = \frac{R(PA) - R(IA)}{1 - R(IA)} \qquad (7.2.1)$$

where R(PA) = Correlation coefficient between the predicted and actual height values

and R(IA) = correlation coefficient between the initial and actual height values.

It is seen from (7.2.1) that if R(PA) is equal to R(IA) then no skill is involved and S is zero. On the other hand, if R(IA) is equal to one then the question of prediction is superfluous.

Another simple skill score that is sometimes used is defined by

$$C = \frac{1}{N} \sum_{i=1}^{N} \frac{|o_i - P_i|}{o_i} \qquad (7.2.2)$$

where P is the predicted value and O represents the observed value. The factor (1-C) thus indicates what fraction of the observed value is indicated by the prediction.

It has to be emphasised, however, that, as in the case of the correlation coefficient, the skill score by itself will not provide a measure of the efficiency of the forecasting technique. It has to be taken in combination with some measure of the stability of the system that is being examined.
For the latter purpose it is convenient to compare the root mean square of the predicted changes, with the root mean square of the observed changes. The root mean square error is defined as

$$\sigma = \left[\frac{\sum_{i=1}^{N} (P_i - O_i)^2}{N} \right]^{\frac{1}{2}} \qquad (7.2.3)$$

where P and O represent predicted and observed values. It is of interest to note that the root mean square error taken by itself would not serve as a good skill score, because it would give the cautious forecaster an opportunity of getting a good score by always playing for the middle of the range.

But, if we used the root mean square errors obtained by using (a) the initial chart as the forecast, and (b) using some other prediction technique,

then a reduction in the root mean square error would indicate positive efficiency for the technique that was employed. This is what is intended by employing a skill score in combination with the correlation coefficient and the root mean square error. To summarise, a verification scheme would require some combination of the following parameters.

a) Correlation coefficient between observed and predicted height changes.

b) Correlation coefficient between predicted and observed height changes, using the initial chart as a forecast.

c) Root mean square error of predicted heights.

d) Root mean square error of predicted heights, using the initial chart as a forecast.

e) Skill score as defined by (7.2.2) or (7.2.3).

As an alternative to (d), the root mean square of observed heights is used by some authors. Comparison with (c) then indicates the efficacy of the forecasting technique. In addition to the above, a number of other parameters, such as, the mean of the maximum positive and negative error in each forecast, have been also used, but their effect can be generally inferred from the basic parameters enumerated above.

The predicted height values at fixed grid points on a map can be also used to make predictions of the geostrophic wind. To assess the accuracy of wind forecasts, we would need a similar verification scheme as required for forecasts of the height. However, in this case it is necessary to determine the root mean square vector error of the wind. An additional parameter, which is sometimes used with wind forecasts, is known as the "k-index". This indicates the spurious build up of kinetic energy caused by errors in the wind forecast. It is given by the formula

$$K = (\overline{P}^2 - \overline{A}^2)^{\frac{1}{2}} \quad , \quad \overline{P}^2 > \overline{A}^2$$
$$= (\overline{A}^2 - \overline{P}^2)^{\frac{1}{2}} \quad , \quad \overline{A}^2 > P^2 \qquad (7.2.4)$$

where $\overline{P}$ and $\overline{A}$ denote the predicted and actual winds, and a bar denotes the mean over a representative area.

7.3 Comparative results of the verification of numerical forecasts.

It may be of interest to quote the results of a few comparative studies of the accuracy of numerical forecasts. A few typical values selected from published results are given below:

The Numerical Prediction Unit at Stockholm (1954) published the results of a verification programme for 25 forecasts made between November 1951 and April 1954. Their mean results were as follows.

TABLE - V

1.	Mean Correlation coefficient between computed and observed 500 mb height changes	0.77
2.	R.M.S. of observed 24 hour changes in metres	121
3.	R.M.S. of computed changes (in metres)	140
4.	Error in computed changes (in metres)	89
5.	Average observed change in metres	8
6.	Average computed change in metres	24

In the United States, a skill score (c) defined as in (7.2.2) was used to test the accuracy of wind forecasts at different intervals between November 1955 to February 1959. Typical values of the factor (1-C) are shown in Table VI.

TABLE - VI

Period	USA	Atlantic	Pacific
Nov. 1955 - Feb. 1956	0.65	0.63	0.77
Nov. 1957 - Feb. 1958	0.68	0.65	0.74
Nov. 1958 - Feb. 1959	0.52	0.52	0.68

On an average, therefore, it could be said that the forecast wind was about two thirds the actual wind.

Wallington (1962) has recently published the results of a verification programme for numerical forecasts with an improved method of smoothing. His figure for 18 hour forecasts of 500 mb contours are shown in Table VII.

TABLE - VII

	Numerical forecast	Persistence forecast
1. R.M.S. height error in decametres.	45	76
2. R.M.S. Vector wind error in knots.	17	28
3. Mean correlation coefficient between forecast and actual change	0.82	—
4. K index	0.82	

Comparatively fewer verification results have been published for graphical integrations. Petterssen (1956) found a mean correlation coefficient of 0.82 between observed and predicted 24 hour height changes of the 1000 mb surface for 10 cyclones in the United States. The predictions were made by graphical integration of Estoque's two parameter model.

5. Preliminary test of the accuracy of charts prepared at NHAC, New Delhi.

At the Northern Hemisphere Analysis Centre, New Delhi, 24 hour 500 mb barotropic prognostic charts have been prepared on a daily basis for a few months The prognosis was made by a modified form of Fjortoft's graphical technique. To get an idea of the accuracy of these charts, a preliminary test was carried out on the charts prepared for the 17 day period from November 1, 1962 to November 17, 1962. The preliminary results of the test may be summarised as follows.

TABLE - VIII

Correlation coefficient between observed and predicted height values at selected grid points.

Lat. ⟶ / Long.	60	45	30
40	0.58	0.59	—*
80	0.79	0.82	0.62
120	0.87	0.54	0.44

Mean = 0.66

* Correlation coefficient not evaluated because of insufficient data.

TABLE IX

Mean difference (in gpm) between observed and predicted height contours at selected grid points

Long. / Lat. →	60	45	30
40	-21	-11	-
80	-55	+30	0
120	-35	- 4	+20

TABLE - X

Maximum and Minimum difference between predicted height values at selected grid points (in gpm) (Entries: Max./Min.)

Lat. ⟶ / Long.	60	45	30
40	-180/0	+ 90/0	-
80	-210/0	+150/0	+70/0
120	-170/0	-140/0	-100/0

TABLE - XI

Standard deviation of observed and predicted height contours (in gpm)

(Entries S.D., Obsd/S.D., Pred.)

Long. \ Lat. ⟶	60	45	30
40	72/60	48/52	—
80	141/116	55/88	37/24
120	98/128	79/66	51/41

In Table VIII we have shown the correlation coefficient between observed and predicted height values at the intersection of different latitude and longitude belts. The mean correlation coefficient was of the order of 0.66, mainly because of low values along 30°N, where the geostrophic assumption becomes less valid. Comparison of tables VIII and IX shows no link between mean difference and the correlation coefficient between observed and predicted height values. High correlations are observed even though the mean difference may be fairly large and vice versa. This is not unexpected, because large differences of opposite sign may cancel each other to give a low mean difference. In Table X, we have shown the maximum and minimum difference between observed and predicted values. The maximum difference, as shown in Table X, was sometimes as high as 200 m, but such occasions were rare. Lastly, Table XI shows that the standard deviation of observed and predicted values were of the same order of magnitude.

It is clearly not possible to draw any firm conclusions from this preliminary test, because we have still to examine the important point, whether these forecasts are significantly better than those obtained on the basis of persistence. Nevertheless, the figures so far have been encouraging.

REFERENCES

1. Petterssen, S. 1957: Tellus, 3, 313-315.

2. Staff Members, Univ. of Stockholm, 1954: Tellus, 2, 139-149.

Chapter 8

Summary and Conclusions

According to PANS-Met, charts used at an aviation meteorological centre should cover an area sufficient to show the meteorological situation likely to affect the flight. At present we provide meteorological service for long distance jet flights, to many parts of the world, but the coverage of upper air data is still not adequate to meet our needs.

The second congress of the W.M.O. has recommended that the basic land stations should be spaced at distances not exceeding 150 km. The spacing between two upper air stations should not exceed 300 km. If in certain desert areas these requirements can not be met, it is now all the more necessary that an attempt should be made to get a coverage as near the desired objective as possible. It is felt that surface stations should not be further apart than 500 km and the spacing between upper air stations should not exceed 1000 km. Even this modest requirement is not fulfilled over large tracts of land and sea. The difficulty arising from lack of data can be partially solved with cooperation from pilots, who may originate more inflight reports, particularly from ocean areas and sparsely populated regions. In this connection, it is also appropriate to stress the need for climatological charts.

The climatological information available at present either in the form of charts or tables does not meet our requirements adequately, as the area covered is generally small and normals for periods less than a month are not available. 5 or 10 day normals of (i) contours of different standard pressure surfaces, (ii) thickness values between different standard pressure levels and (iii) temperature and winds upto 100 mb would be extremely useful. The percentage frequency of various types of weather hazards, such as, thunderstorm, duststorm, fog etc. for 5 or 10 day periods will be also helpful to the forecaster. Climatological information is also needed on jet streams, mountain

waves, dense cirrus data etc.

Planning for long distance operations requires considerable advance preparation, including the study of meteorological conditions over the route, We need to know not only average conditions, but also extremes. This information is essential for assessing items, such as, the fuel load and the overall pay load. Information about the terrain and the extreme values of temperature and pressure enables the operator to estimate the lowest safety flight level over a particular route. A prior study of the climatology of the area covered by the route gives the pilot and the navigator an idea of the weather conditions likely to be encountered during the flight.

For the benefit of pilots and forecasters, climatological summaries have been prepared by the Indian Meteorological Service for all scheduled routes over India and neighbouring countries. These summaries contain information on

i) physical features of the route,

ii) seasonal synoptic characteristics affecting the route, including mean rainfall, mean surface temperature and mean surface pressure in different sectors,

iii) cloudiness, with the height of the base and top of clouds,

iv) frequency of rainy days, thunderstorms and fog,

v) surface and upper winds upto 12 km and

vi) mean freezing level and icing conditions.

Climatological information regarding simultaneous occurrence of adverse weather conditions (justifying SPECI conditions) at all major airfields in India and designated alternates has been also compiled by India Meteorological Department on the basis of 5 years data. This information is very useful for the purpose of diversion in the event of bad weather over the destination airport.

Progress in civil aviation holds out prospects of an accelerated rate of growth in the years to come. In December 1961, the General Assembly of the United Nations passed a resolution on the peaceful uses of outer space of which one section was on the study of atmospheric sciences. For further study on this subject a few advanced countries have launched weather satellites and high altitude rockets in the past few years. These new tools for meteorological research have immense possibilities and will probably provide the data required for the coming generation of supersonic commercial aircraft.

DIAGRAMS

FIG.1 THE UNIT GRID

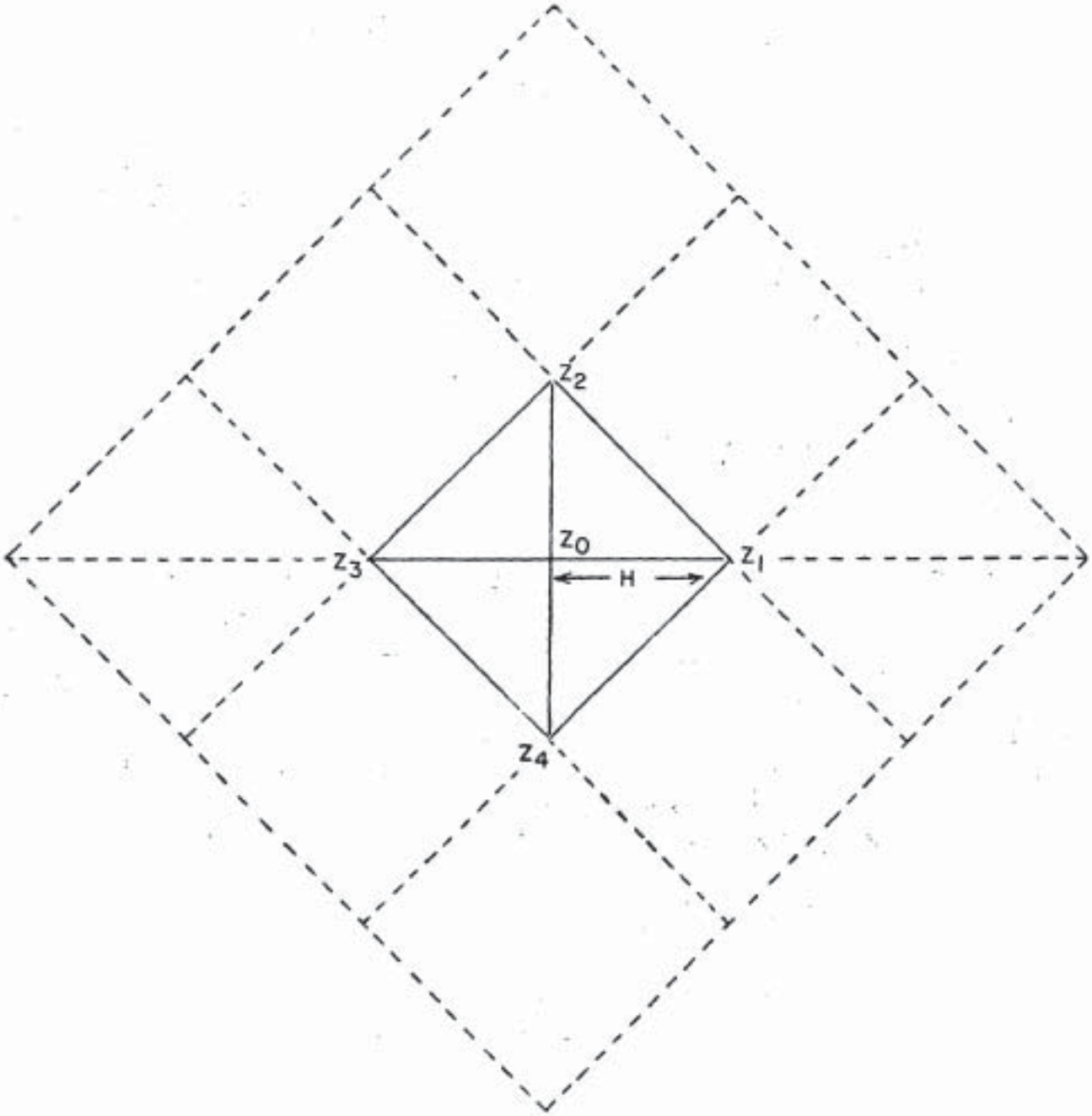

FIG. 2

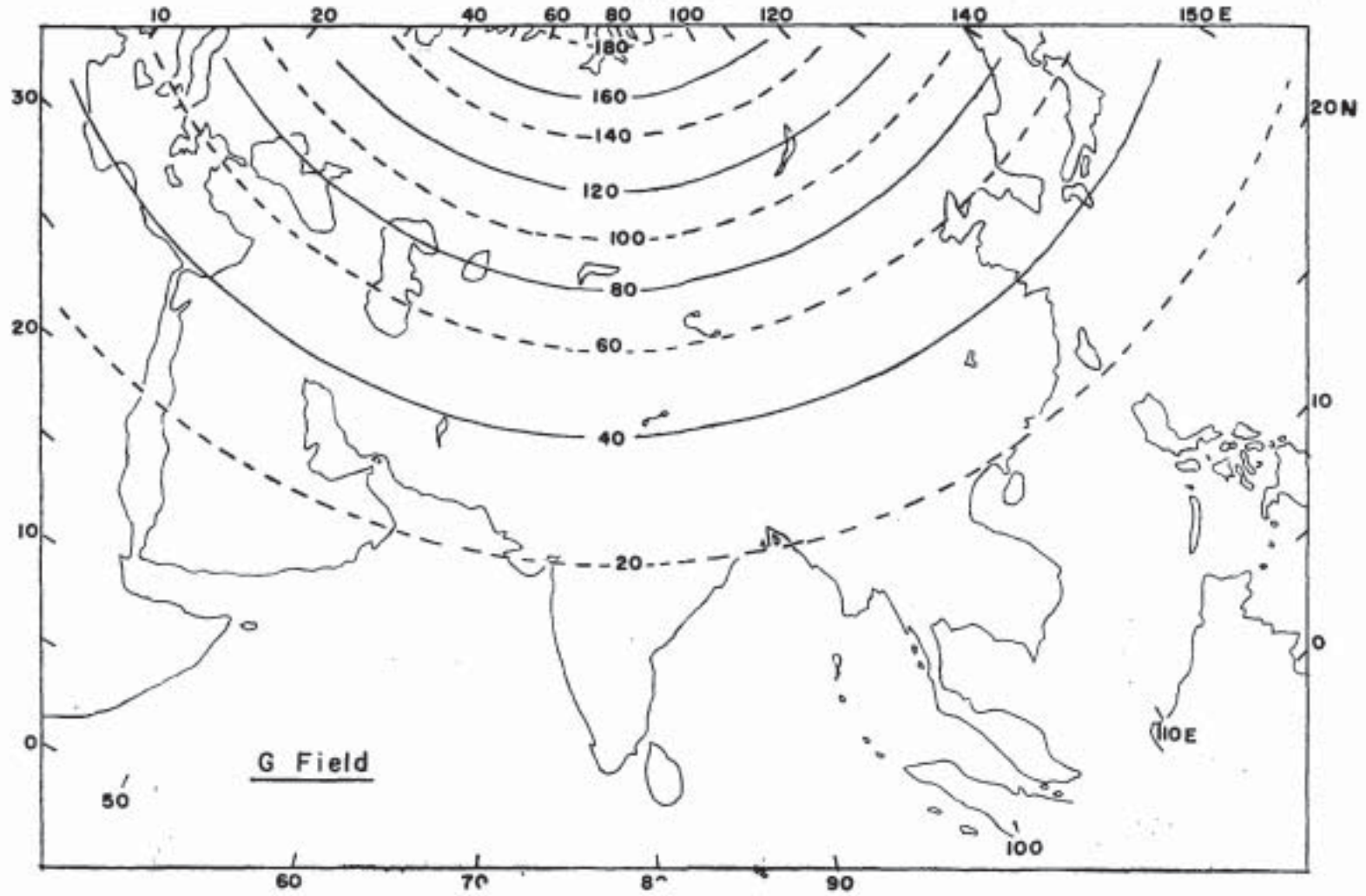
10
20
40
60
80
100
120
140
150 E
180
160
140
120
100
80
60
40
20
30
20
10
0
20N
10
0
G Field
50
60
70
80
90
100
110E

FIG. 3

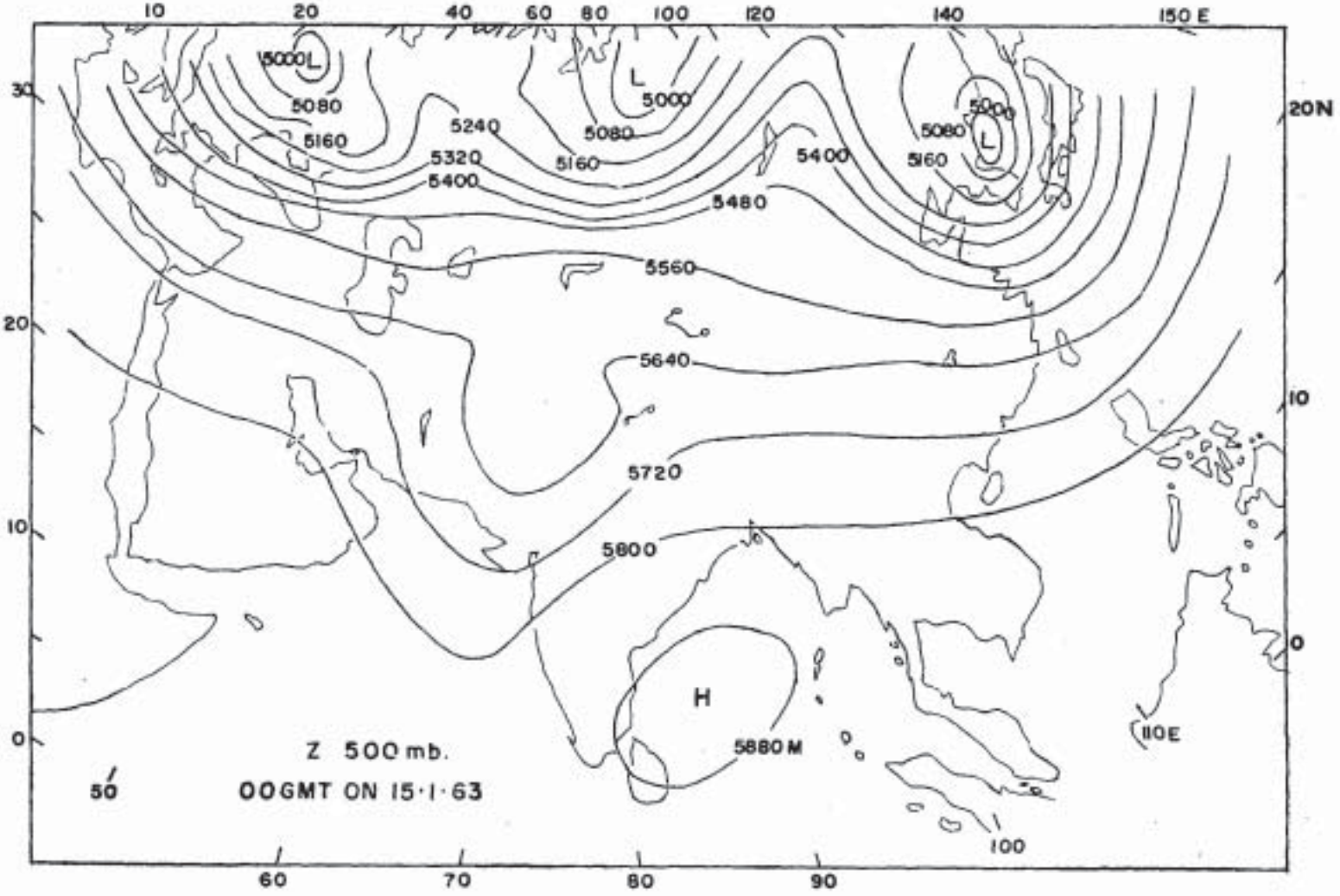
10
20
40
60
80
100
120
140
150 E
30
20
10
0
20N
10
0
15000L
5080
5160
5240
5320
5400
L
5000
5080
5160
5480
5560
5640
5720
5800
5000
5080
5160
5400
H
5880M
Z 500mb.
00GMT ON 15·1·63
50
110E
100
60
70
80
90

FIG. 4

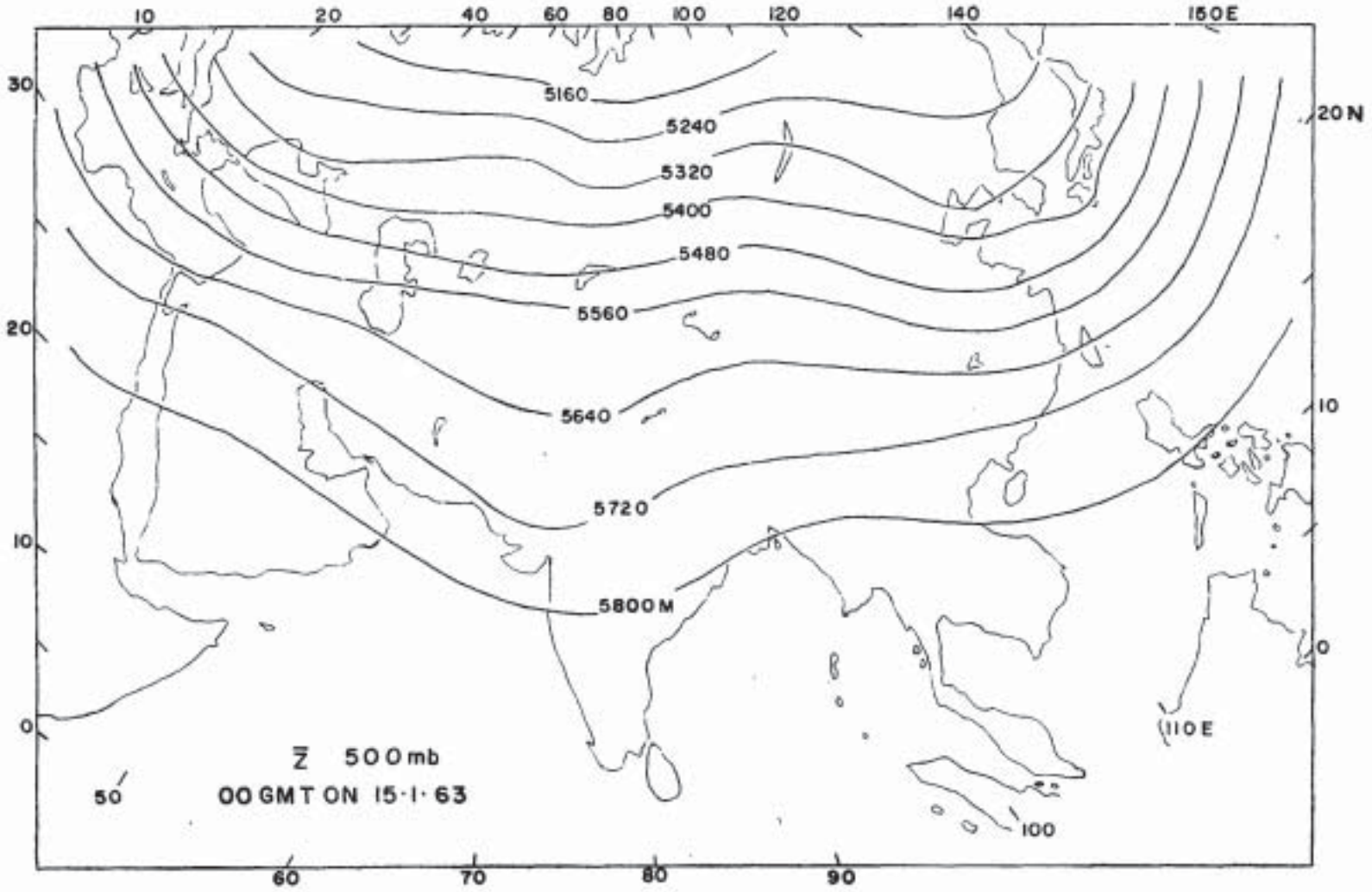
10
20
40
60
80
100
120
140
150E
30
20
10
0
20N
10
0
5160
5240
5320
5400
5480
5560
5640
5720
5800M
110E
100
50
60
70
80
90
$\bar{Z}$ 500mb
00 GMT ON 15·1·63

FIG. 5

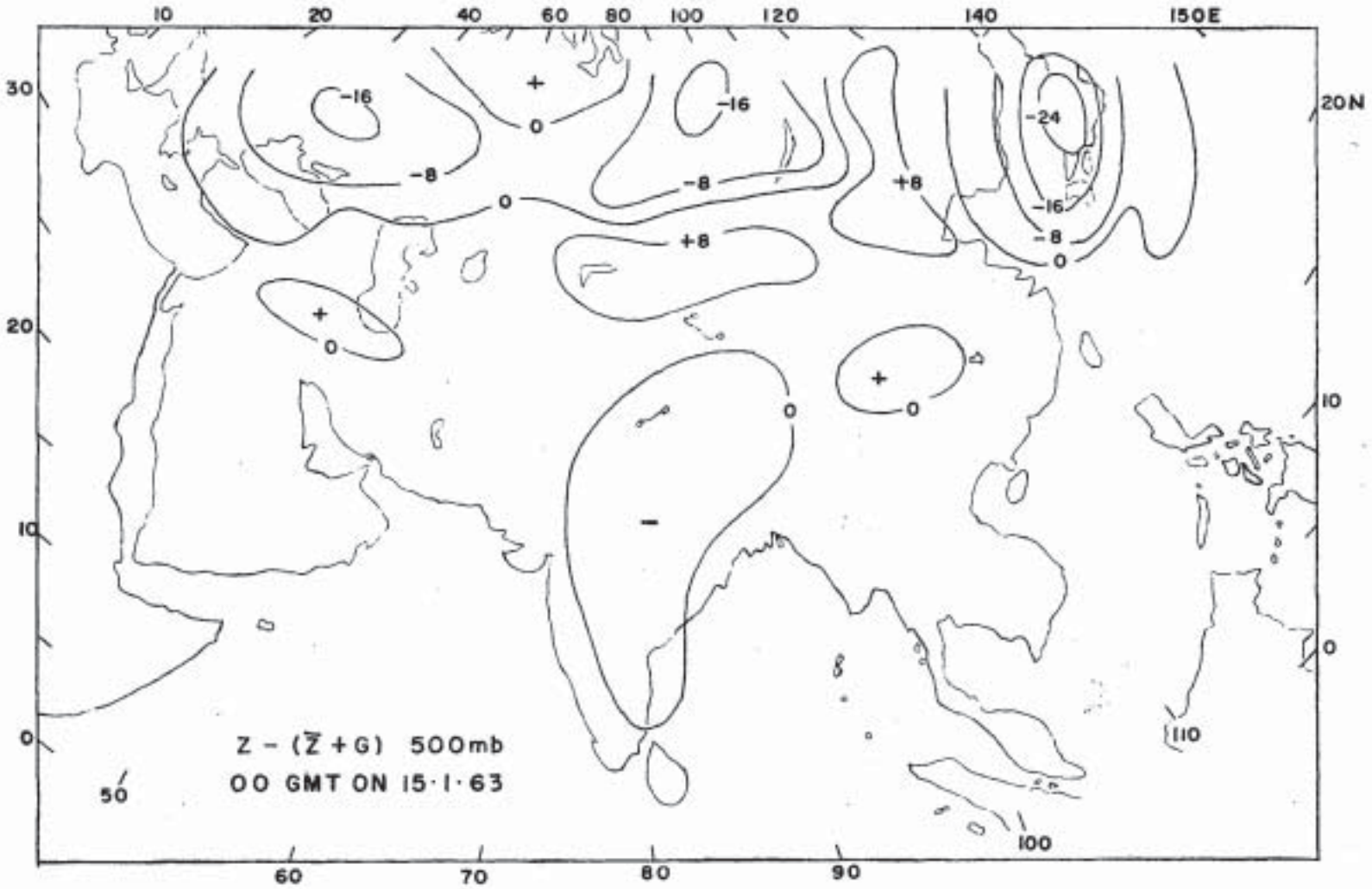
10
20
40
60
80
100
120
140
150E
30
20
10
0
20N
10
0
-16
+
0
-16
-24
-8
-8
+8
0
-16
-8
0
+8
+
0
+
0
0
-
110
100
50
60
70
80
90
Z - (Z̄ + G) 500mb
00 GMT ON 15·1·63

FIG. 6

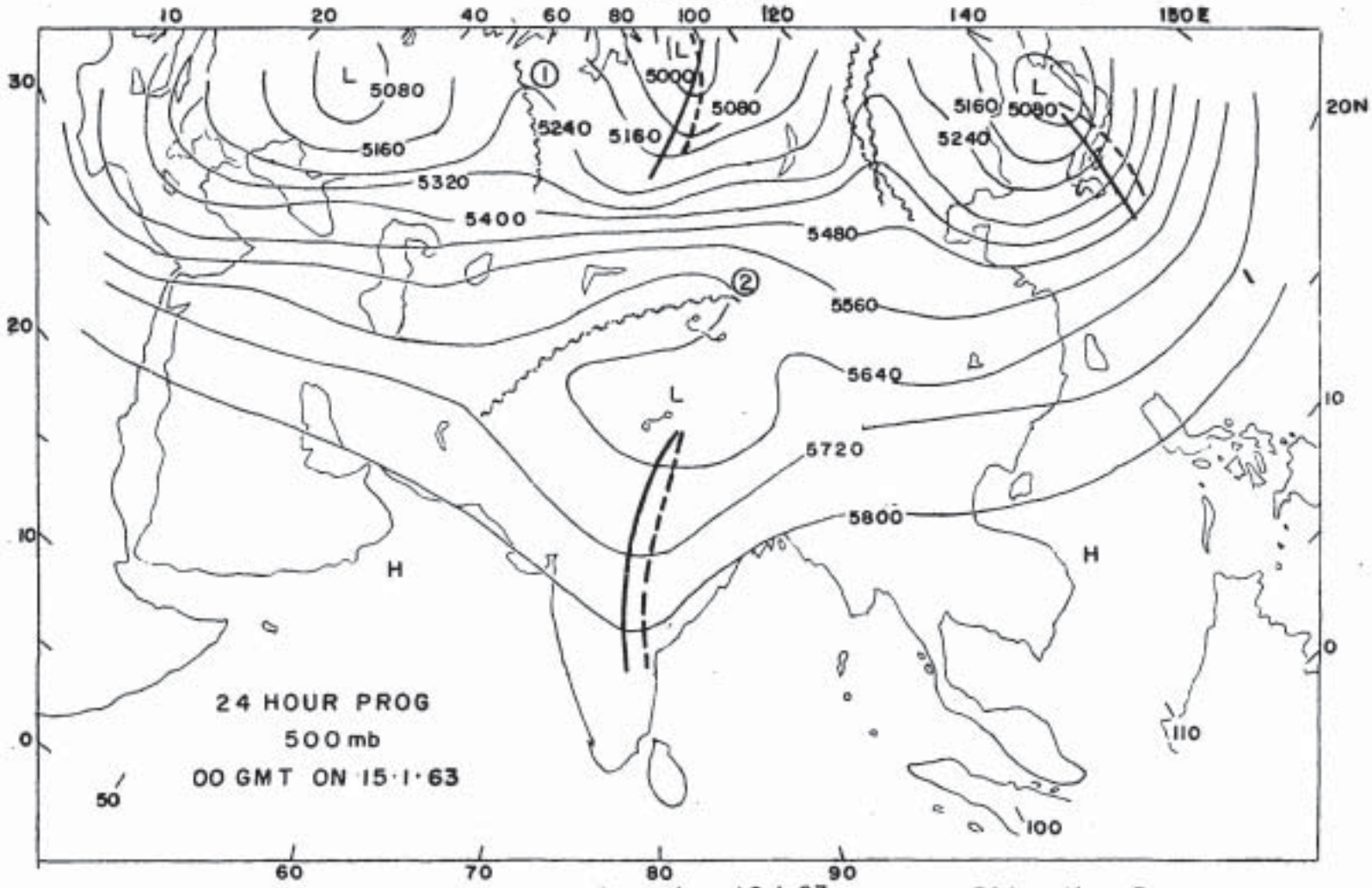

Trough line Prog. ---- Trough line Actual on 16·1·63 ~~~~ Ridge line Prog.
~~~~ Ridge line Actual on 16·1·63 At 1 & 2 Ridge lines on Prog & Actual 00Z of 16·1·63 are practically coincident.
~~~~

FIG. 7

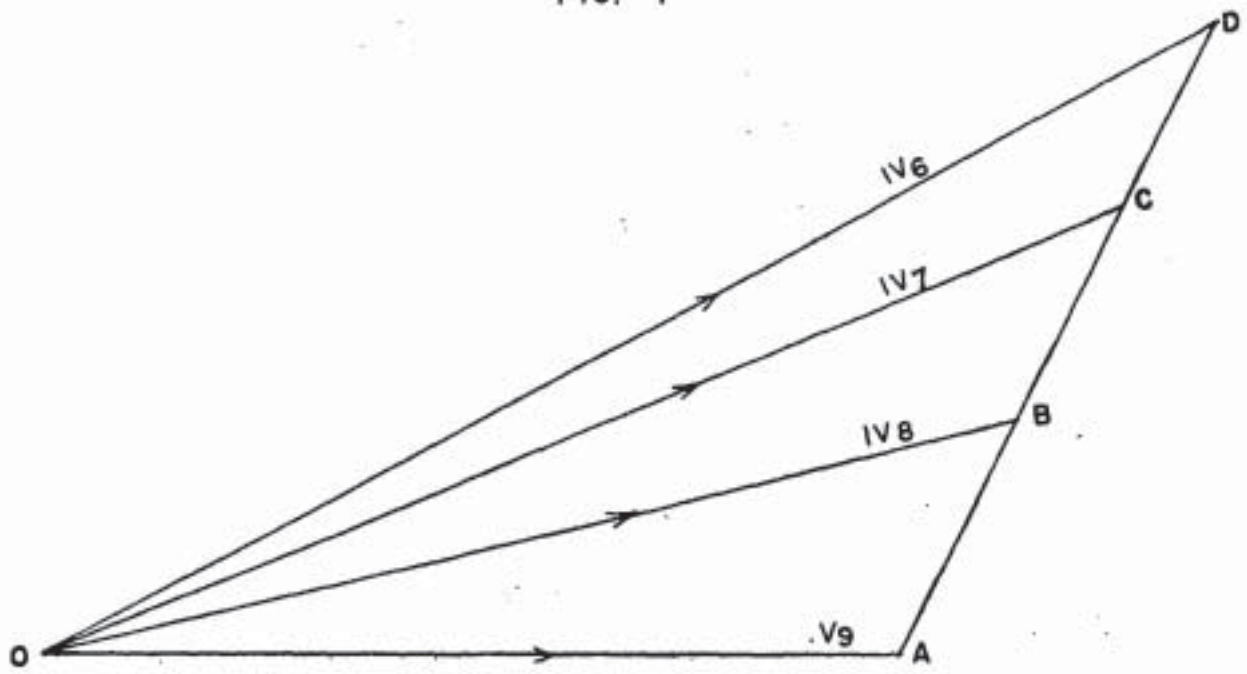

FIG. 8

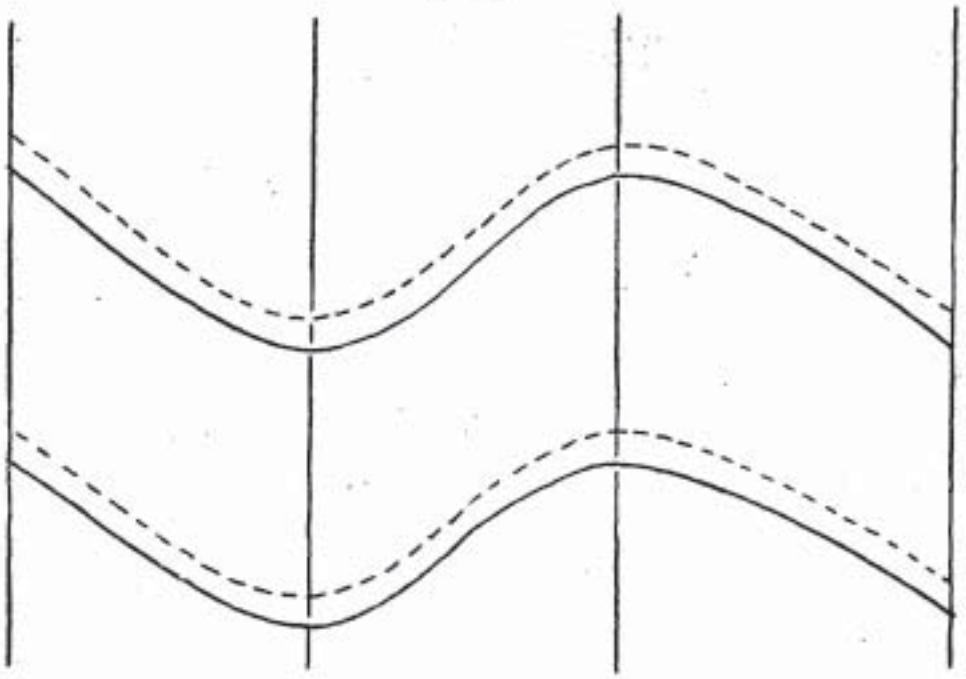

Isotherms are indicated by dotted lines. Full lines indicate contours.

FIG. 9

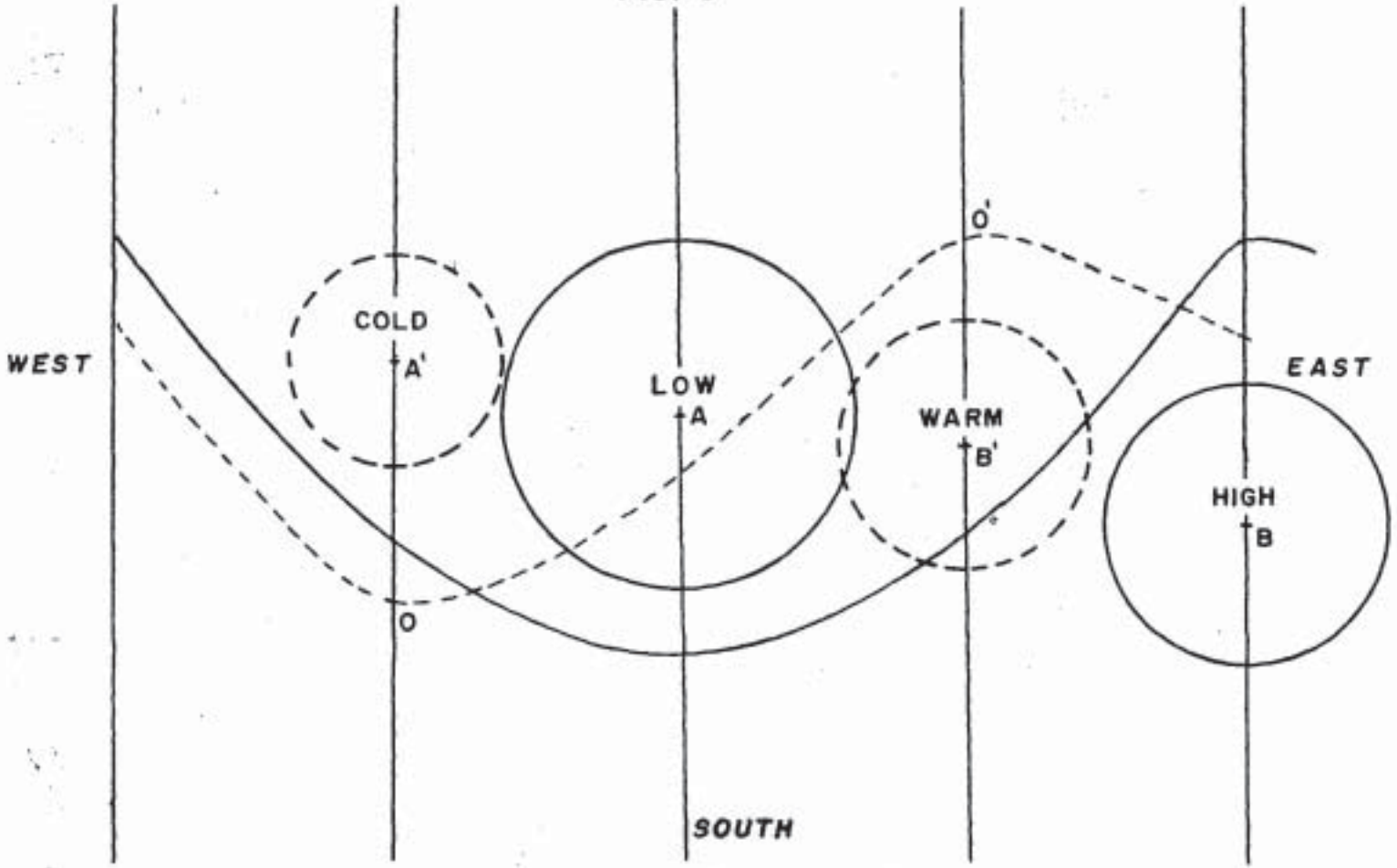

Isotherms are indicated by dotted lines. Full lines indicate contours

No. III – 4.1	Discussion of Typical Synoptic Weather Situations : Weather over the Indian Seas during the Post-Monsoon Seas – V. Srinivasan and K. Ramamurthy.
No. IV-13	Rainfall of India – P. Jagannathan.
No. IV-16	Microseisms and Weather – A.N. Tandon and S.N. Bhattachar
No. IV-17	Medium Range Forecasting – K.R. Saha and D.A. Mooley.
No. IV-18.1	On the Criteria for declaring the onset of the southwest monsoon over Kerala – R. Ananthakrishnan, U.R. Acharya ar A.R. Ramakrishnan.
No. IV-18.2	Monsoons of India: Synoptic Features associated with ons of Southwest Monsoon over Kerala – R. Ananthakrishnan, V. Srinivasan, A.R. Ramakrishnan and R. Jambunathan.
No. IV-18.3	Some aspects of the "Break" in the Indian Southwest Monso during July and August – K. Ramamurthy.
No. IV-18.4	Northeast Monsoon – V. Srinivasan and K. Ramamurthy.
No. IV-20	Evaporation – N. Ramalingam.
No. V-I	Techniques of High Level Analysis and Prognosis : 1. Organization and Methods of Analysis – P.K. Das, N.C. Rai Sircar and D.V. Rao.